RADIATION EXPERIMENTS ON COSMOS 2044: K-7-41, PARTS A, B, C, D, E

A. L. Frank, E. V. Benton, E. R. Benton
Physics Research Laboratory
University of San Francisco
San Francisco, California 94117, USA

V. E. Dudkin, A. M. Marenny
Institute of Biomedical Problems
76a Khoroshevskoye shosse
Moscow 123007, USSR

FINAL REPORT
USF-TR-76
4 September 1990

Work partially supported by NASA Grants Nos. NCC2-521 (NASA-Ames Research Center) and NAG9-235 (Johnson Space Center, Houston).

Principal Investigator: E. V. Benton, University of San Francisco

TABLE OF CONTENTS

RADIATION EXPERIMENTS ON COSMOS 2044: K-7-41 PARTS A, B, C, D, E

Abstract

The Cosmos 2044 biosatellite mission offered the opportunity for radiation measurements under conditions which are seldom available (an inclination of 82.3° and altitude of 294 × 216 km). Measurements were made on the outside of the spacecraft under near-zero shielding conditions. Also, this mission was the first in which active temperature recorders (the ATR-4) were flown to record the temperature profiles of detector stacks. Measurements made on this mission provide a comparison and test for modeling of depth doses and LET spectra for orbital parameters previously unavailable. Tissue absorbed doses from 3480 rad (252 rad/d) down to 0.115 rad (8.33 mrad/d) were measured at different depths (0.0146 and 3.20 g/cm^2, respectively) with averaged TLD readings. The LET spectra yielded maximum and minimum values of integral flux of 27.3×10^{-4} and 3.05×10^{-4} cm^{-2}s^{-1}sr^{-1}, of dose rate of 7.01 and 1.20 mrad/d, and of dose equivalent rate of 53.8 and 11.6 mrem/d, for $LET_\infty\cdot H_2O \geq 4$ keV/μm. Neutron measurements yielded 0.018 mrem/d in the thermal region, 0.25 mrem/d in the resonance region and 3.3 mrem/d in the high energy region. The TLD depth dose and LET spectra have been compared with calculations from the modeling codes. The agreement is good but some further refinements are in order. In comparing measurements on Cosmos 2044 with those from previous Cosmos missions (orbital inclinations of 62.8°) there is a greater spread (maximum to minimum) in depth doses and an increased contribution from GCRs, and higher LET particles, in the heavy particle fluxes.

INTRODUCTION

The Cosmos 2044 mission was the latest of five Soviet biosatellite missions in which the University of San Francisco has participated. The previous missions were Cosmos Nos. 782, 936, 1129 and 1887 /Peterson et al., 1978; Benton et al., 1978a, 1978b, 1981, 1988; Kovalev et al., 1981/. Previous work which applies to radiation measurements in space also covers a wide range of U.S. space flights, including the Gemini, Apollo, Skylab, Apollo-Soyuz and Space Shuttle missions /Benton et al., 1977a, 1977b; Benton and Henke, 1983; Benton, 1984; Benton et al, 1985; Benton, 1986; Benton and Parnell, 1987/.

The Cosmos biosatellites have been host to a wide variety of space biology and radiation experiments performed by international research groups. Radiation dosimetry and spectrometry experiments are typically included for the purpose of providing radiation measurements specific to the mission and to implement long-range goals of mapping radiation intensities in near-earth orbit and of providing measured comparisons for the radiation modeling codes. The Cosmos missions also offer the opportunity to intercompare measurements with other research groups and in this way compare measurements of certain quantities (i.e. dose, LET) using different techniques.

The Cosmos 2044 biosatellite mission took place between September 15 and 29, 1989, for a duration of 13.8 days. The orbit was elliptical, with minimum and maximum altitudes of 216 km and 294 km, respectively, and an inclination of 82.3°. The selection of international experiments on the flight included K-7-41 from the University of San Francisco. This experiment was composed of five parts (A through E) for the purpose of measuring (A) depth dose distribution in thermoluminescent detector (TLD) stacks under very low shielding, (B) LET spectra of HZE particles under low shielding, with stacks composed of plastic nuclear track detectors (PNTD) and emulsions, (C) high energy neutron and proton fluxes with ^{59}Co activation foils, (D) high energy neutron fluxes with ^{232}Th fission foils and (E) thermal and resonance neutron fluxes with ^{6}LiF foils. The measurements will be used to determine radiation levels for the special orbital parameters of this mission and will be compared with calculations from radiation modelling codes.

EXPERIMENTS

The five parts of the experiment K-7-41 are discussed individually below.

Part A

The objective of this experiment was to measure the depth dose under very thin shielding on the outside of the spacecraft and to determine what fraction of the dose was due to low energy electrons versus heavy charged particles. This required that the shielding of the outermost detectors be no more than a few mg/cm^2 and that the detectors themselves also be very thin (because of the short ranges of the particles). The maximum depth in the TLD stacks was 3.2 g/cm^2. Although computer codes exist for calculating doses encountered in LEO both from protons and electrons, there have been only a few instances where a direct comparison (under very thin shielding) has been possible between experiment and theoretical prediction. The orbit of Cosmos 2044 will allow the codes to be compared for parameters quite different from any for previous flights.

The TLD stacks were placed in cylindrical holders (Fig. 1) which were then arrayed in plates attached to the outside of the spacecraft. Three TLD stacks were placed in each of four mounting plates (B9-1, -2, -3, -4) for a total of twelve flight stacks. The TLDs and all other detectors mounted on the outside of the spacecraft were held in "clam-shell" style containers which were closed before re-entry to prevent heating of the detectors in the atmosphere. Some detectors and two containers are shown in Fig. 2.

Each stack was composed of both thin (0.02395 g/cm^2 thickness) and thick (0.2322 g/cm^2 thickness) TLD-700 extruded chips. Thin TLDs were used to a depth of 0.5175 g/cm^2 and thick TLDs at greater depths. A double window of 7.5 μm thick Kapton polyimide films, both aluminized to an optical density of 3, held the TLDs in place and shielded them from sun and space. In the depth-dose results, the mass density of the Kapton (0.00213 g/cm^2) has been converted to an equivalent mass density of ^{7}LiF (0.00266 g/cm^2) on the basis of low energy proton ranges.

Part B

The objective here was to measure the low energy, heavy particle (excluding electrons) LET spectra under very low shielding (outside the spacecraft)

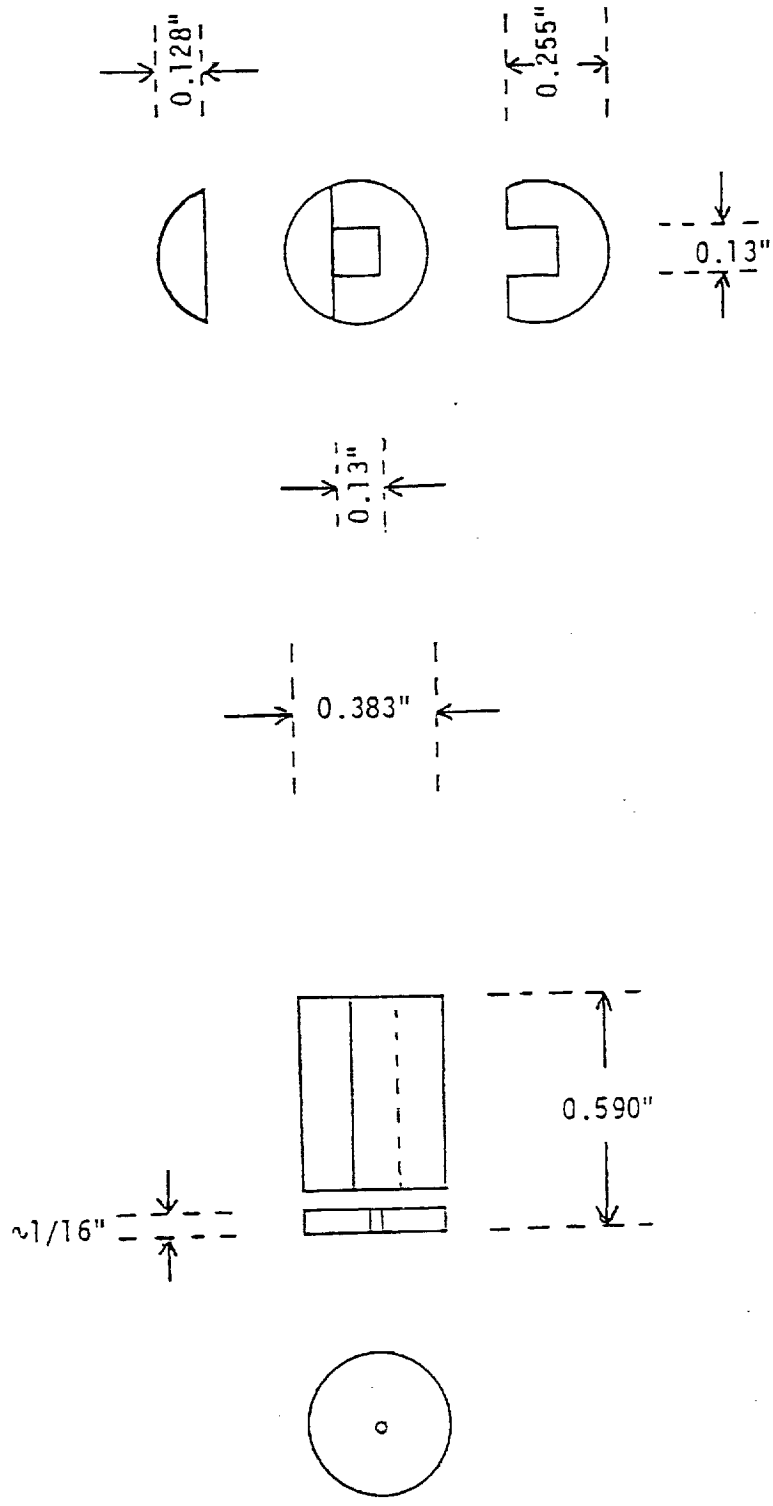

Fig. 1. Sketch of a TLD stack holder for K-7-41A, made of acrylate. Three stacks were placed in each of four plates (Plate No. B9-1, -2, -3, -4) for a total of twelve flight stacks (outside the spacecraft). A double window of aluminized Kapton polyimide (total thickness: 15 μm) separated the stacks from space.

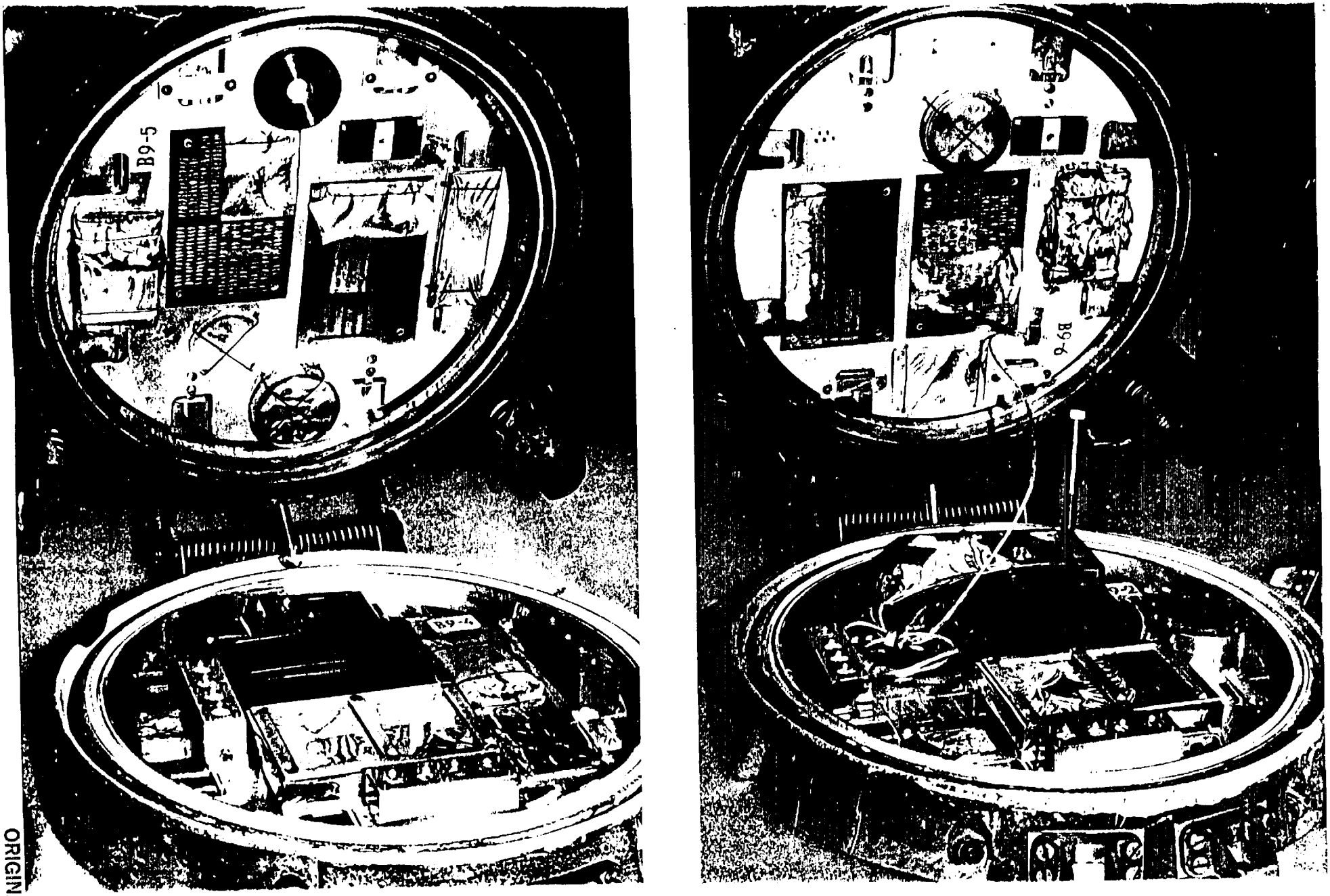

Fig. 2. Photograph of Cosmos 2044 "Clam-Shell" type containers for mission dosimeters. The containers were mounted on the outside of the spacecraft.

and as a function of depth. Although there have been some previous measurements of let spectra under such conditions, the orbital dependence and the effects of solar cycle on the low energy charged particle component are still not well understood. The very high inclination orbit of Cosmos 2044 (82.3°) will provide a test of radiation models in the polar regions, which has not been possible before.

The hardware consisted of two hermetically sealed flight units containing PNTD and nuclear emulsion stacks and with aluminized Kapton double-windows, as in Part A. The PNTD stacks were 3 cm in diameter and included sets of CR-39 and Cronar polyester detectors. The emulsion stacks were enclosed in thin stainless steel cylinders of the same diameters. The physical configurations of the units and stacks are shown in Figs. 3 and 4. The flight units were placed outside the spacecraft with F1 being in Plate B9-2 and F2 in Plate B9-1.

In addition to the radiation detector stacks, these units also held temperature sensors for the ATR-4 Ambient Temperature Recorder which has been developed by NASA for spacecraft use (NASA, 1989). This system allows a time-temperature profile to be determined for each sensor included on the mission (up to eight sensors). This is an important consideration for flight materials, such as some of the radiation detectors, which are heat sensitive.

Part C

Here the intent was to obtain some information on the neutron energy spectra. The detectors were located both on the outside and inside of the spacecraft.

The outside experiment consisted of two flight units containing ^{59}Co activation foils and PNTD films. An aluminum frame with aluminized Kapton double-windows was placed above the detectors but the sides of the units were open to vacuum. The PNTDs used were Cronar polyester. The purpose of the PNTDs in this experiment was for an intercomparison between those open to vacuum and those hermetically sealed. Due to space limitations, CR-39 was not included. The configuration of the units is shown in Fig. 5. The flight placement of the detectors was F1 in Plate B9-4 and F2 in Plate B9-3.

The inside detector consisted of a single ^{59}Co activation foil. In conjunction with the activation foil was a stack of nuclear emulsions to provide a comparison with the emulsions exposed on the outside of the spacecraft in

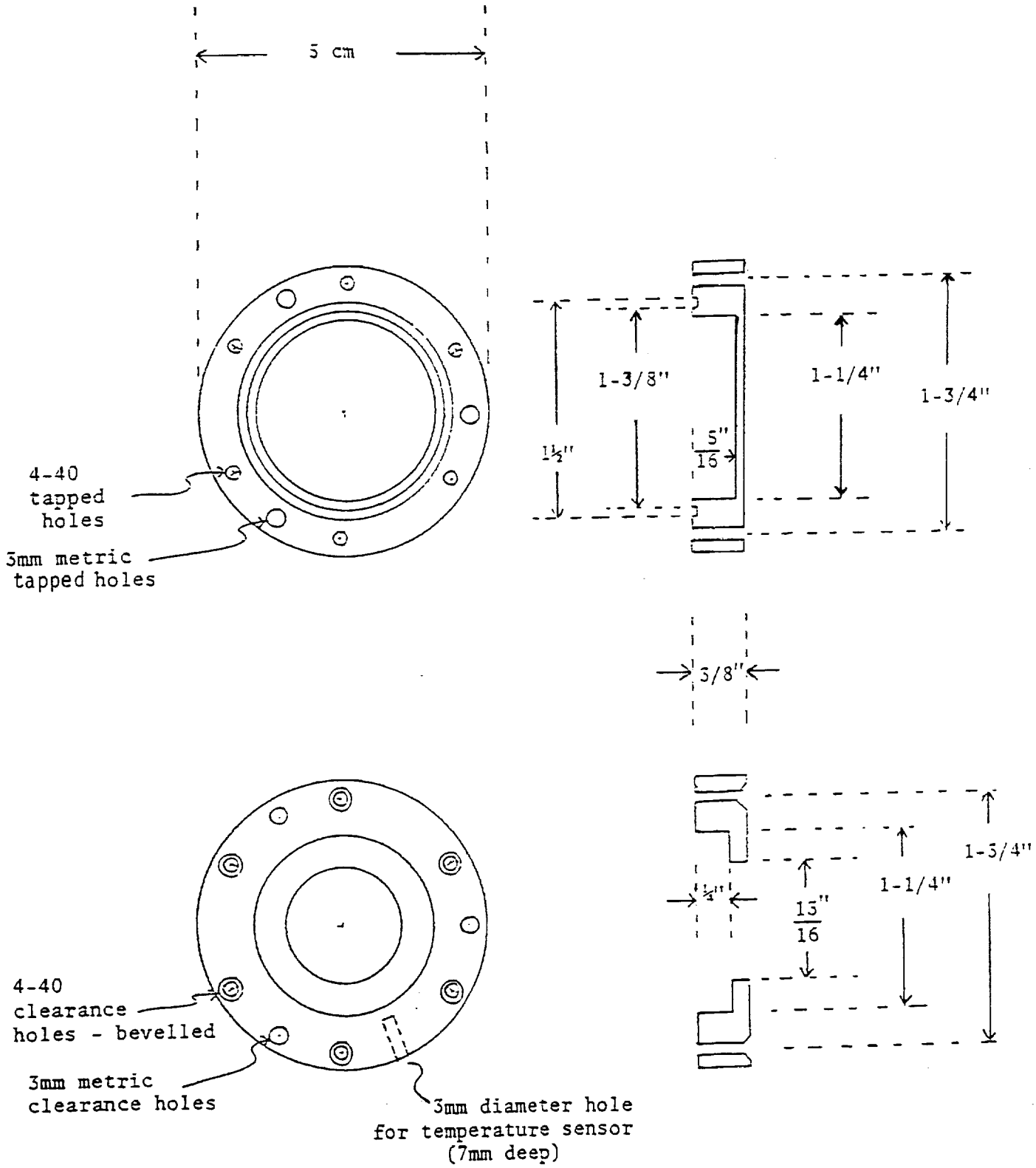

Fig. 3. Sketch of an aluminum container with O-ring seal for the plastic and emulsion stacks in K-7-41B. There were two flight units, F1 and F2 (outside the spacecraft). A double window of aluminized Kapton polyimide (total thickness: 15 μm) separated the stacks from space.

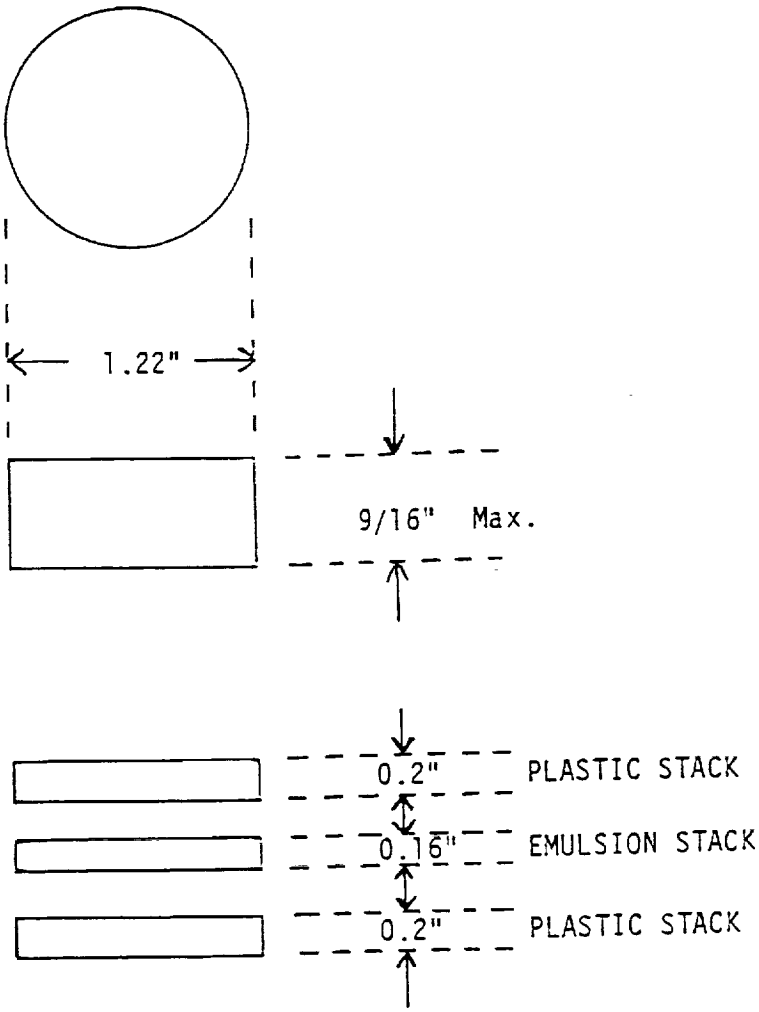

Fig. 4. Sketch of the plastic and emulsion stacks for K-7-418

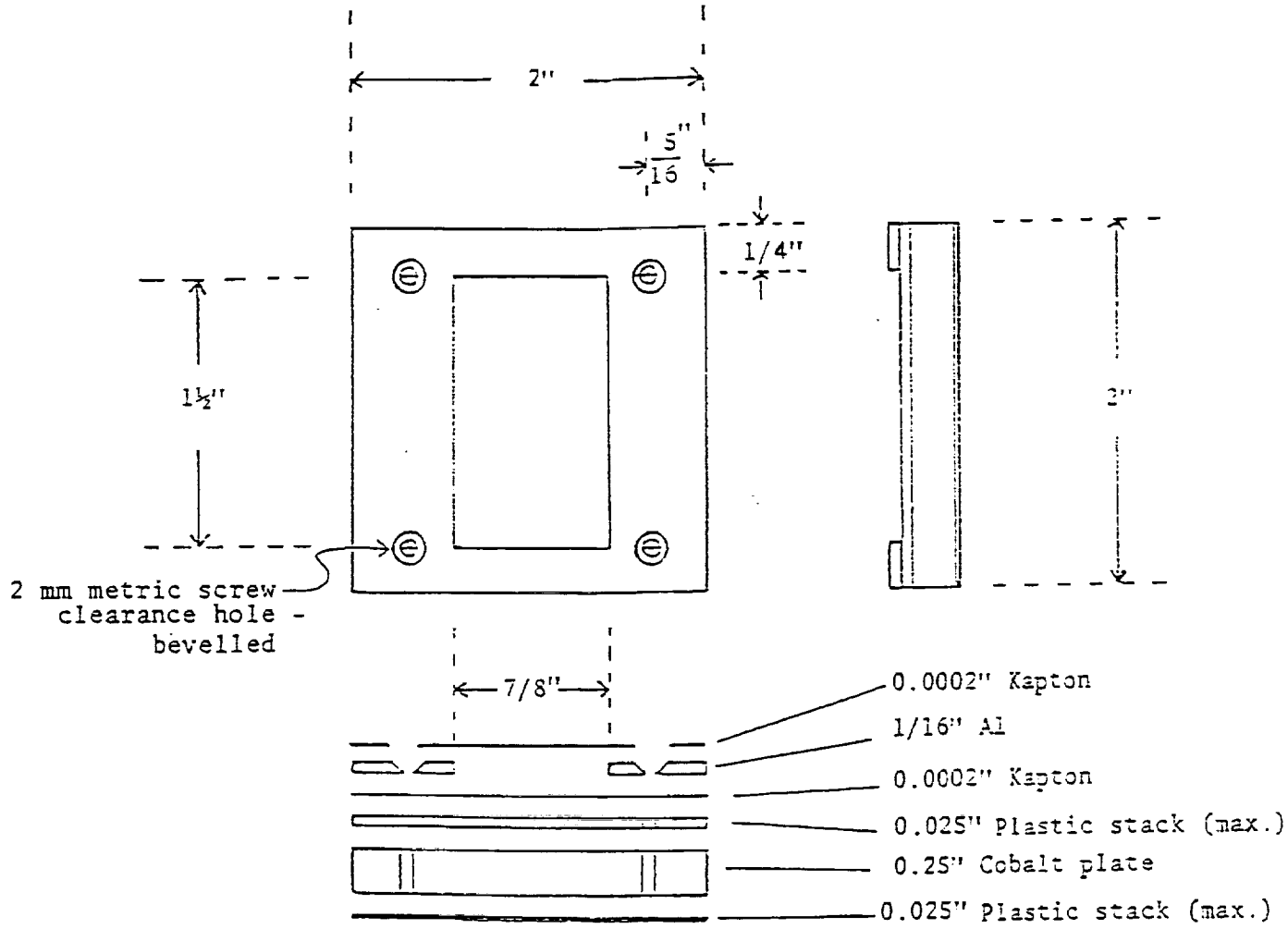

Fig. 5. Sketch of the ^{59}Co activation foil detector units for K-7-41C, two of which were placed outside the spacecraft. A third activation foil with an emulsion stack was placed inside the spacecraft.

Part B. The selection of available isotopes with suitable activation cross sections and decay product half-lives for spaceflights of a few days places severe limitations on this method. Cross sections exist for the measurement of both low energy (thermal plus resonance) and high energy (>10 MeV) neutrons, with some proton contribution, with the activations forming ^{60}Co and ^{58}Co. However, readout requires a very sensitive, low background spectrometer.

Part D

The goal of this part was to measure high energy (>1 MeV) neutron fluxes and dose equivalent rates averaged over the mission duration. The detectors were fission foils of ^{232}Th in conjunction with solid state nuclear track detectors (SSNTDs) of muscovite mica. There were two flight units (F1 and F2) and each unit was composed of four ^{232}Th foils with mica (1.27 cm in diameter) in an aluminum and Lexan polycarbonate holder (see Fig. 6). The arrangement of the foils was mica/^{232}Th/mica and lead discs of 0.5 mm thickness were placed to each side for reduction of radiation from the ^{232}Th foils. The flight units were mounted on the outside of the spacecraft, with F1 in Plate B9-8 and F2 in Plate B9-7.

Part E

The goal here was to measure the thermal ($\leq$ 0.2 eV) and resonance (0.2 eV $< E_n <$ 1 MeV) neutron fluxes and dose equivalent rates averaged over the mission duration. The detectors were layers of ^{6}LiF (TLD-600) in conjunction with CR-39 PNTDs. There were two flight units and each unit was composed of two ^{6}LiF layers with CR-39 (1.27 $\times$ 1.27 cm) in an aluminum and Lexan polycarbonate holder (see Fig. 7). The arrangement of the components was CR-39/^{6}LiF/CR-39 with Gd foil of 0.0025 cm thickness around one of the two detectors. The Gd foil absorbs thermal neutrons and allows a separation of thermal and resonance neutrons. The flight units were mounted on the outside of the spacecraft, with F1 in Plate B9-5 and F2 in Plate B9-6.

Processing and Readout of Detectors

a) Temperature Profile and Environmental Conditions During the Cosmos 2044 Mission

The exposed Cosmos 2044 detectors were returned to this laboratory on 12 October 1989, or thirteen days after satellite re-entry. The condition

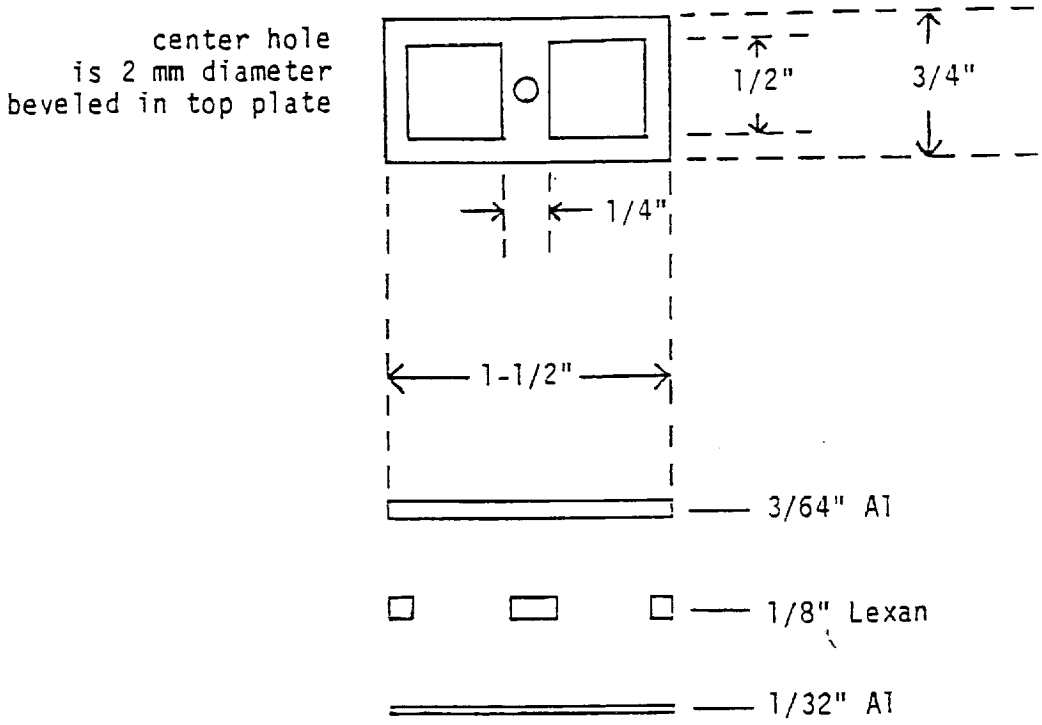

Fig. 7. Sketch of the ^{6}LiF/CR-39 neutron detector holders for K-7-41E. Each unit contained one unshielded detector and one shielded by 25 μm-thick Gd foil. Two units (F1 and F2) were placed outside the spacecraft.

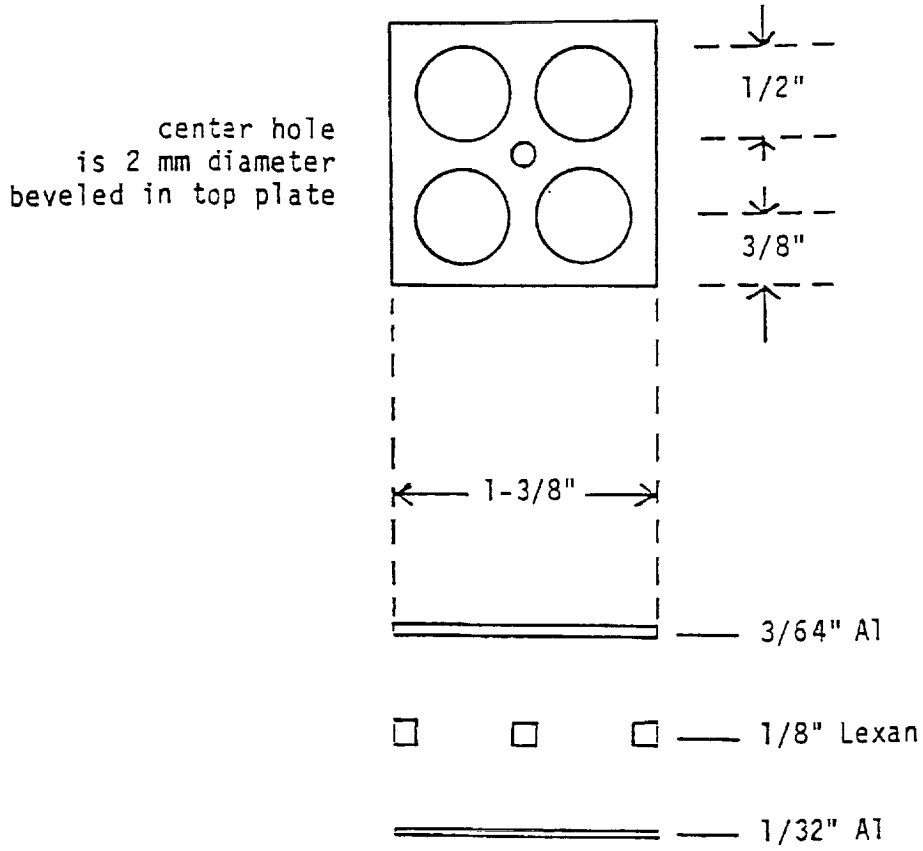

Fig. 6. Sketch of the ^{232}Th fission foil detector holders for K-7-41D. Two units, F1 and F2, were placed outside the spacecraft.

of the flight units appeared generally good, with the possible exception of the sealed PNTD/emulsion stack units (Part B) where the outer Kapton windows were found to be easily flexed. This was due to tiny perforations, apparently from micrometeorite impacts, causing the windows to lose their vacuum seals. It was subsequently determined that the inner windows were not perforated and that the flight units retained their air during the mission. This is important to the response of the PNTDs where a deficiency of oxygen results in faded or unformed latent particle tracks.

Temperature Measurement

During the mission, the temperature profiles were measured by two ATR-4 Ambient Temperature Recorders (NASA, 1989). Each of these devices had four temperature sensors which were distributed over plates containing flight dosimeters (Plates B9-2 and B9-6 in the KHA-1 clamshell container and Plates B9-1 and B9-7 in the KHA-3 container). The two aluminum canisters used in the K-7-41B experiment each had a sensor embedded in the side and sealed with a high-temperature conducting epoxy. The sensors were accurate to $\pm$ 0.5°C over the temperature range from -40° to +60°C. Temperature readings were taken from each sensor at intervals of 3.75 min.

In Fig. 8 is the temperature record of the sensor in the K-7-41B F1 canister. Aside from some brief temperature spikes the variation was between 3° and 36°C with an average of about 22°C. Based on environmental studies of the PNTDs and TLDs, no measureable effect on detector response would be expected from this temperature profile. The closure of the clamshell containers about a day before landing, as the spacecraft began moving into the outer atmosphere, is obvious from the drop in temperature.

In Fig. 9 is the temperature record of the sensor in the B F2 canister. The temperature profile is similar to, but about 5°C less than, the profile for F1 up to the last day. As the spacecraft began moving into the upper atmosphere prior to landing, the clamshell container (KHA-3) did not close. Where the F1 sensor temperature decreased, that of F2 increased to above 50°C and then spiked to above 60°C during the landing. Based on environmental studies for a more extended period of time, these temperatures could have affected the PNTD response, but because of the brevity of the conditions there was no measurable effect. The PNTDs from F1 and F2 were intercompared after the processing.

After disassembly of the flight units, the detectors were processed and

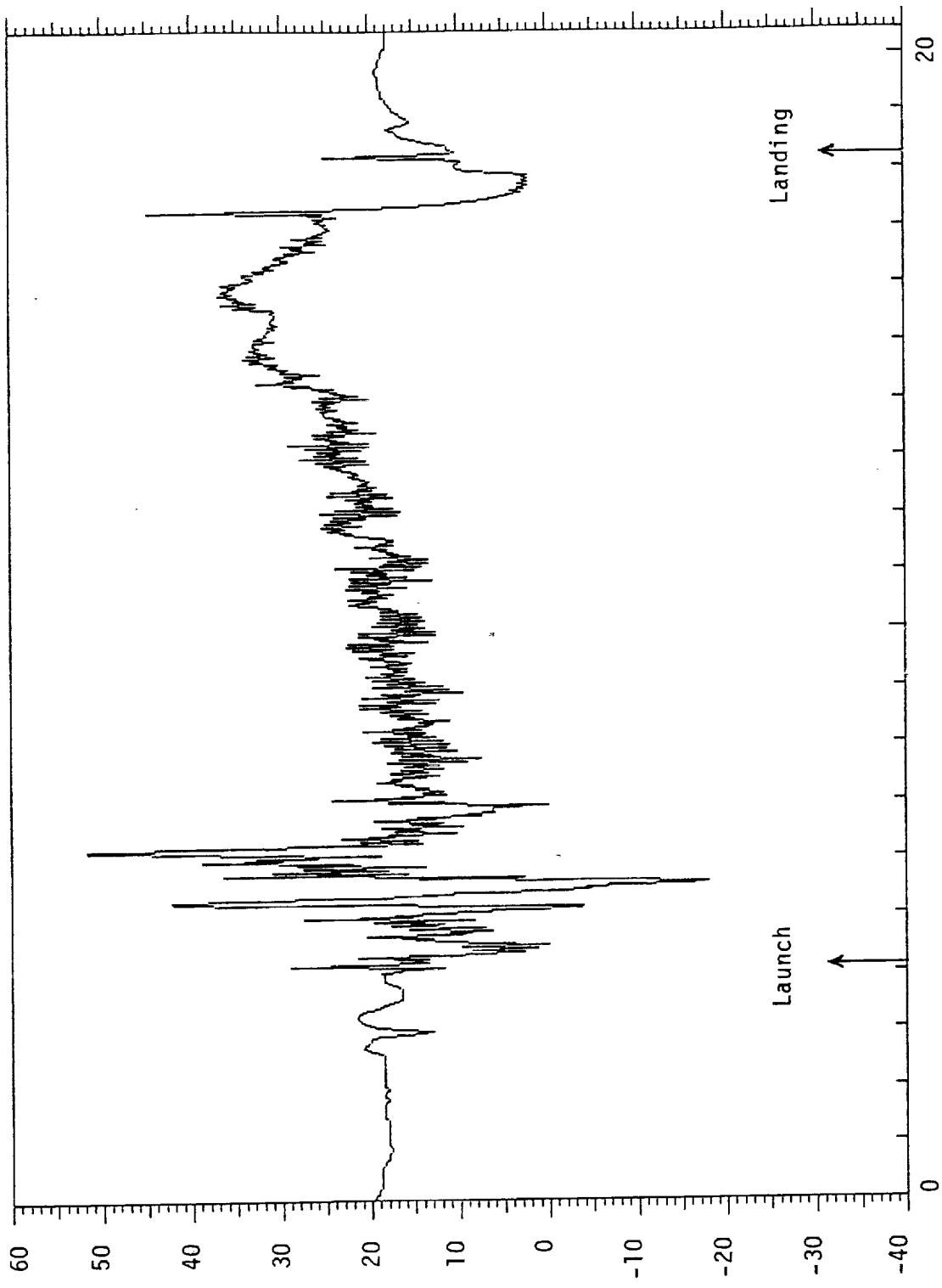

Fig. 8. Record of ATR-4 temperature probe embedded in the K-7-41B F1 canister (Plate B9-2; Container KHA-1).

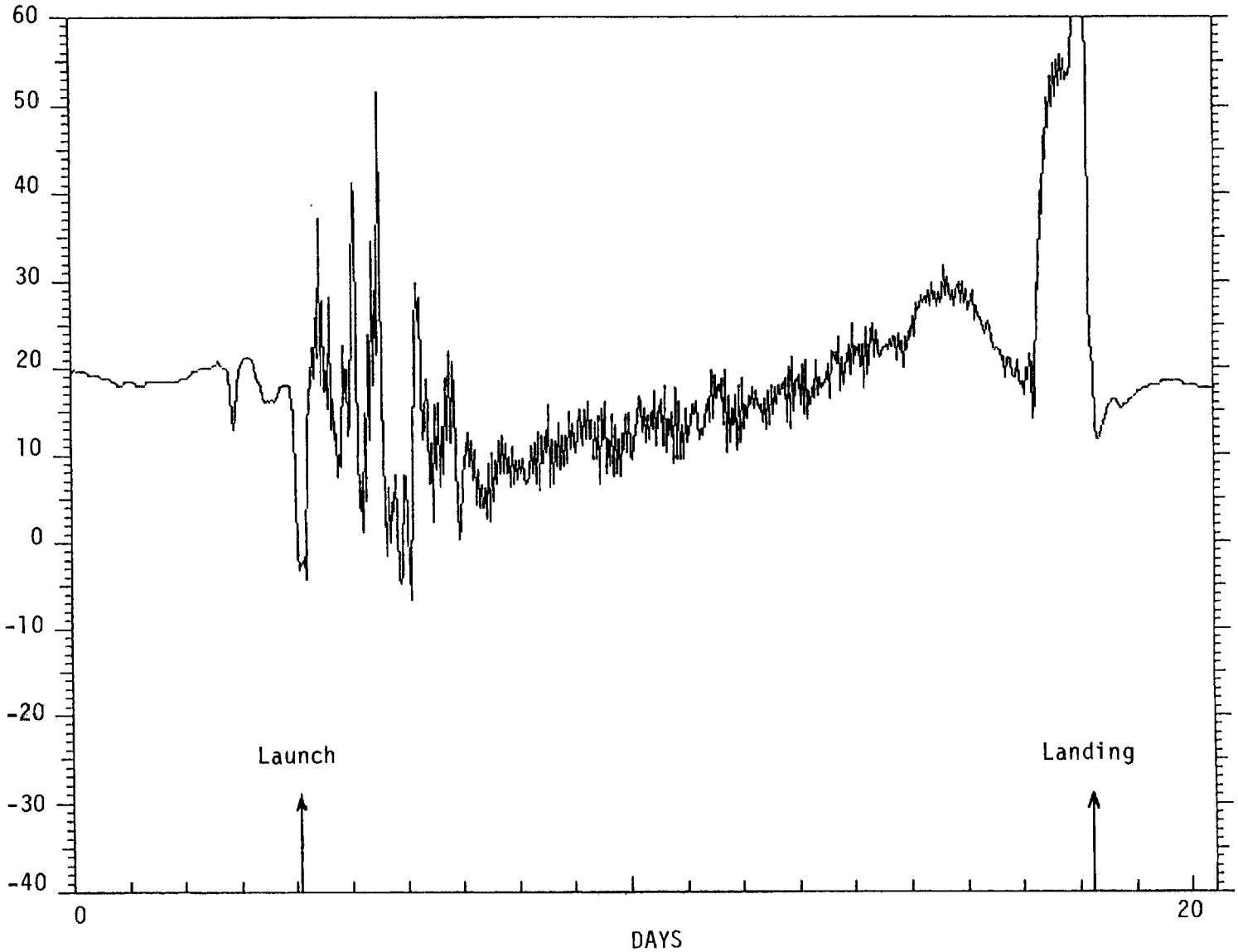

Fig. 9. Record of ATR-4 temperature probe embedded in the K-7-41B F2 canister (Plate B9-1; Container KHA-3).

read out as follows:

b) TLD Readout

The TLDs (TLD-700) were read out on Harshaw Model 2000 and 4000 Readers. In each case glow peak integrated current was measured between 120° and 250°C. In addition, the glow peak curves were recorded up to 325°C with the Model 4000 Reader. Flight, background and standard exposures were read out together for both the thin and thick TLDs. Standard exposures of 1 rad from a ^{137}Cs source were employed and TLD calibrations extending up to 10^4 rad were used to correct for the supralinear high dose response of the least shielded TLDs (Fig. 10). All flight TLD readings were then corrected for background and converted to tissue rad doses.

c) PNTD Processing and Readout

The CR-39 PNTDs were processed in 6.25 N NaOH solution at 50°C for 7 days. The bulk etch, B (thickness removed from a single surface), was measured for each film. Pairs of detectors were reassembled in their flight orientations and the two inner, adjacent surfaces were scanned under an optical microscope. This enabled the particles to be separated into short range (SR): matching tracks appearing on only the two interior surfaces, and long range, galactic cosmic rays (GCR): matching tracks appearing on all four surfaces of the pair of films. The SR particles include short-range secondary particles from target nuclei within the plastic and stopping primary galactic and trapped particles. All protons are registered as SR particles because of their short registration range in CR-39. The GCR particles include both primary GCRs and the long-range secondaries which are mainly the projectile fragments of GCRs. The major and minor axes of the elliptical surface openings of tracks were measured. The axial measurements, together with the B of the samples and the calibrated LET response function of the CR-39 material, were then used to generate particle LET spectra.

d) Nuclear Photographic Emulsions

The nuclear emulsions (Fuji types 6B and 7B) have been processed by standard techniques and are being read out at Marshall Space Flight Center, Huntsville.

e) $^{59}C0$ Activation Foils

Immediately after arrival, the ^{59}Co foils were transferred to Dr. A. Smith of Lawrence Berkeley Laboratory (LBL) to be read out at a highly shielded

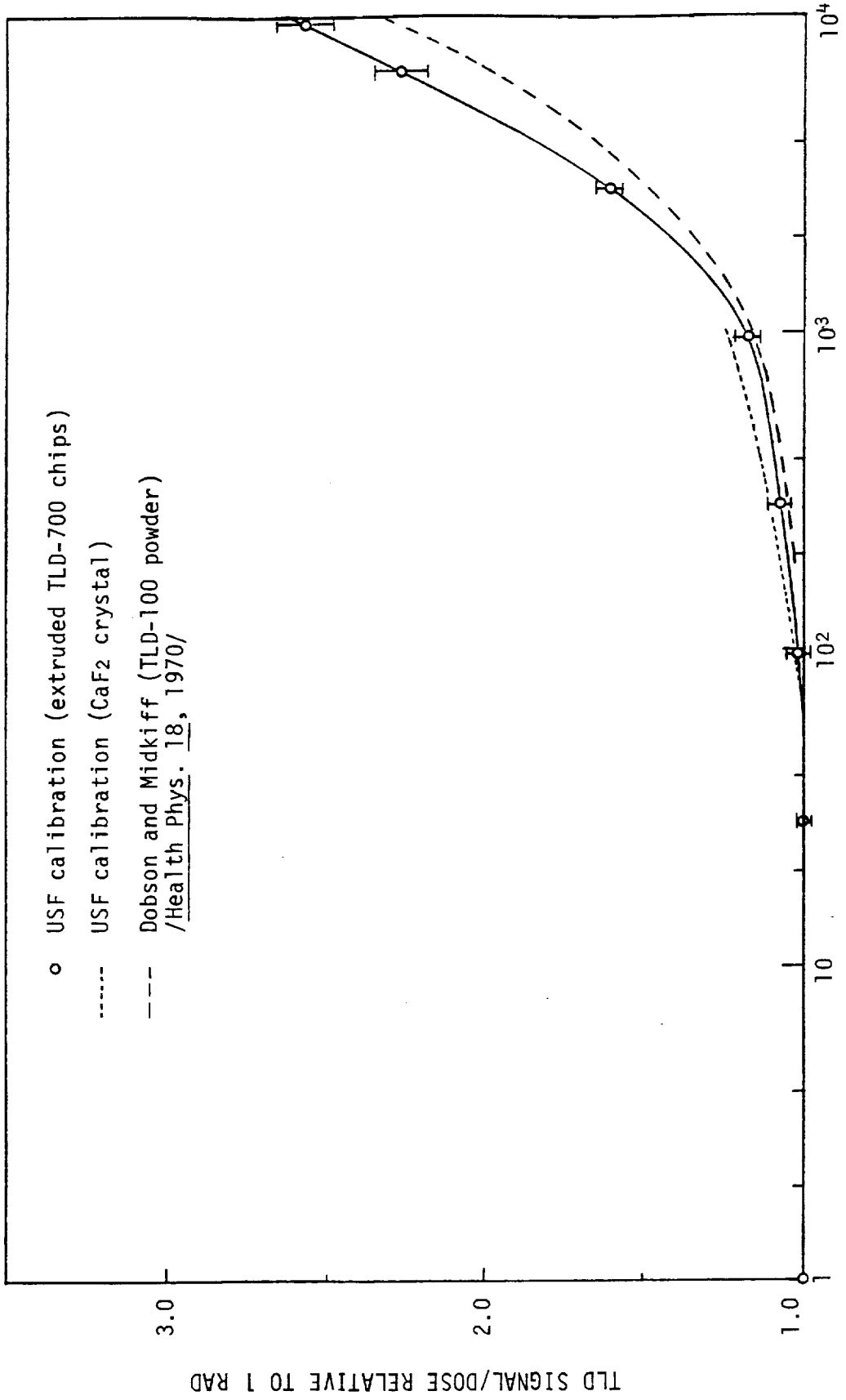

Fig. 10. TLD calibration showing the high-dose supralinearity found in TLD-700 extruded chips. The data from Dobson and Midkiff /1970/ (TLD-100 powder) was typical of LiF supralinearity reported.

site with high efficiency Ge(Li) detectors. The data analysis and background studies for these measurements are still in progress.

f) ^{232}Th/Mica Detectors

The muscovite mica discs from these detectors were processed for 2 hr at 21°C in 50% HF acid. They had been processed for 5 hr under the same conditions pre-flight to develop the fossil fission tracks to large size. The flight tracks on the discs were then counted under an optical microscope. Backgrounds were counted using the backs of the flight discs. Detector calibrations based on fission cross sections for neutrons and protons and assumed spectral distributions for neutrons and protons were used to convert track densities into neutron fluences (see Benton et al., 1978a). Dose equivalents were determined using Quality Factors (QF) of 10.

g) ^{6}LiF /CR-39 Detectors

The CR-39 films from these detectors were processed in 6.25 N NaOH solution at 70°C for 5 hr. Track densities were counted on the surfaces both adjacent to and opposite to the ^{6}LiF layers in order to determine net alpha particle track densities from the ^{6}Li(n,α) T reaction. The ground control detectors were used to measure the non-flight alpha particle backgrounds. Since there were CR-39 films on both the space and spacecraft sides of the ^{6}LiF layers, the average track densities on the two films yielded a measure of 4π neutron incidence.

In each flight unit, one detector was covered with 0.0025 cm-thick Gd foil and one was not. The thermal neutron absorbance of the Gd gives an effective low energy cutoff of 0.2 eV for the covered detectors. By subtraction the measured track densities were separated into those due to neutrons below and above 0.2 eV.

The flight background track densities, counted on the backs of the CR-39 detectors, were quite large and also depth dependent. Since the front and back of the detectors were at different depths, it was necessary to interpolate between only two measured points to obtain the appropriate backgrounds. Consequently, the measurement accuracy is somewhat less than implied by the associated standard deviations which were calculated from counting statistics. In addition, the neutron spectra assumed in the calibrations are the completely thermalized distribution below the Gd cutoff and a 1/E distribution above. Deviations of the flight spectra from these assumptions will also contribute to measurement error.

RESULTS

Part A

The average depth dose rates for the three TLD stacks in each of the four flight plates are plotted in Figs. 11, 12, 13 and 14. The measurements show more than a 4 order-of-magnitude decrease in dose rate down to 3 g/cm^2 depth. The average plate dose rates are given in Table 1. The total flight doses for the twelve TLD stacks are given in Tables 2a, -b, -c and -d. It can be seen that there are shielding differences for the various stacks. As an example, three individual TLD stack distributions for Plate No. B9-3 are shown in Fig. 15. Stack No. 1 dose rates are clearly less than Stacks Nos. 3 and 9. There are substantial variations at the tops of the stacks, as seen in Tables 2a–2d (2040 rad for No. 2 up to 4480 rad for No. 9) while stacks Nos. 1, 5 and 10 have smaller doses at the maximum depths than do the others.

Part B

The CR-39 PNTDs have been given the standard processing for 7 days in 6.25 *N* NaOH solution at 50°C. Adjacent pairs from the flight stacks were reassembled, scanned and measured with a microscope and electronic micrometer. The particle tracks were separated into galactic cosmic rays (GCR), which traversed all four surfaces of the CR-39 pair, and short range (SR), which traversed only the two inner surfaces or the two inner surfaces plus one outer surface of the pair. The GCRs are mainly galactic cosmic rays or their projectile fragments where $Z \geq 2$. Anomalous particles may also contribute to the four-surface tracks. The SR tracks are mainly short range secondary particles or primary protons near their stopping points. The short registration range of protons in CR-39 makes four-surface proton tracks very low-probability events. GCR stopping particles of $Z \geq 2$ can contribute to SR tracks, but this also has a low probability.

Five sets of integral LET spectra (Total, GCR and SR) from the PNTD stack in the F1 canister are given in Figures 16–20. Four sets of spectra from the F2 canister are given in Figures 21–24. The minimum to maximum shielding is covered in each PNTD stack. The minimum shielding is greater for F1 because the least shielded CR-39 layer was damaged on one surface by the high electron dose encountered. An extra layer of thin plastic protected the least shielded CR-39 layer in F2.

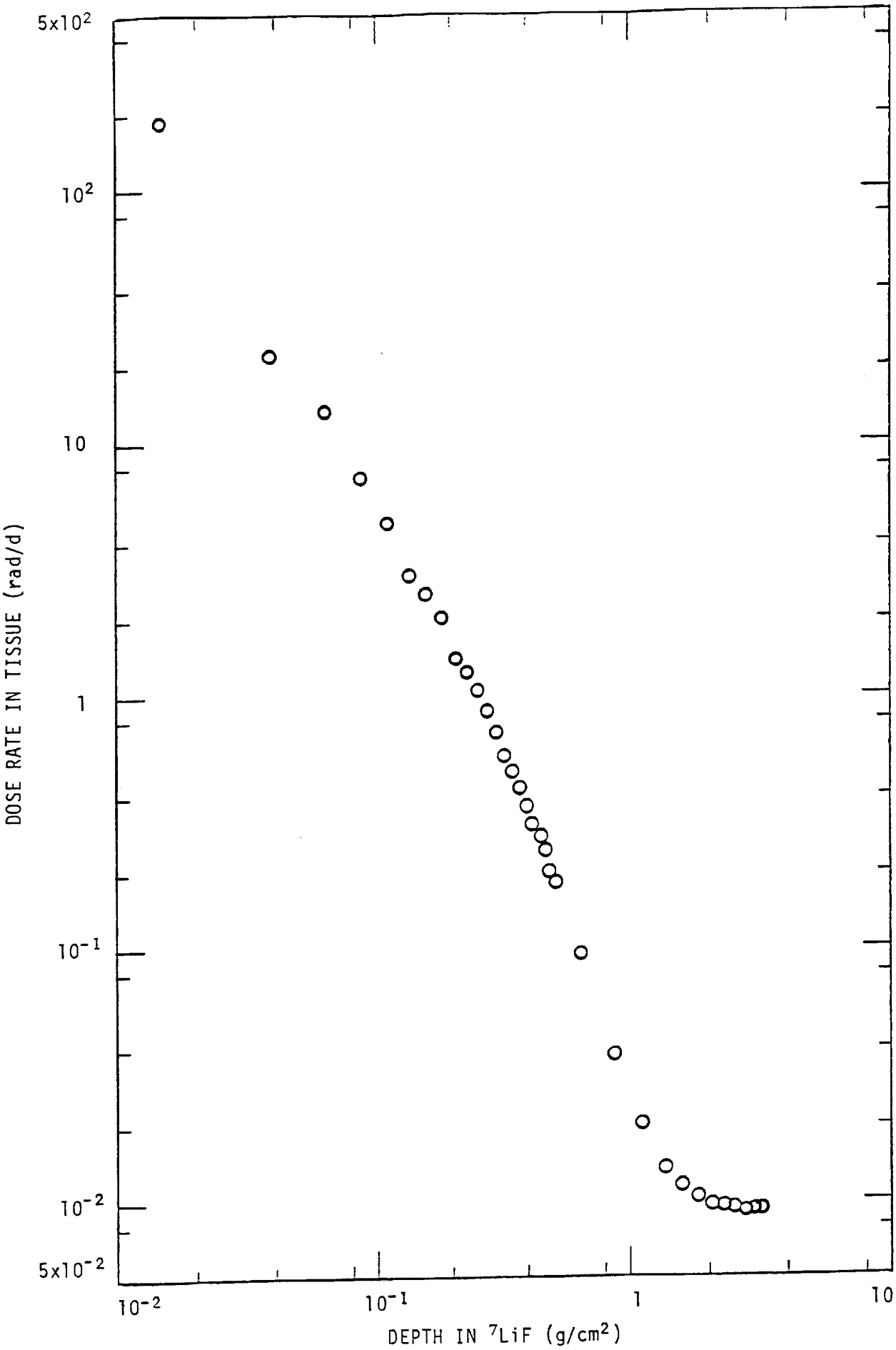

Fig. 11. Average dose rates in Plate No. B9-1 (TLD stacks Nos. 4, 8, 12)

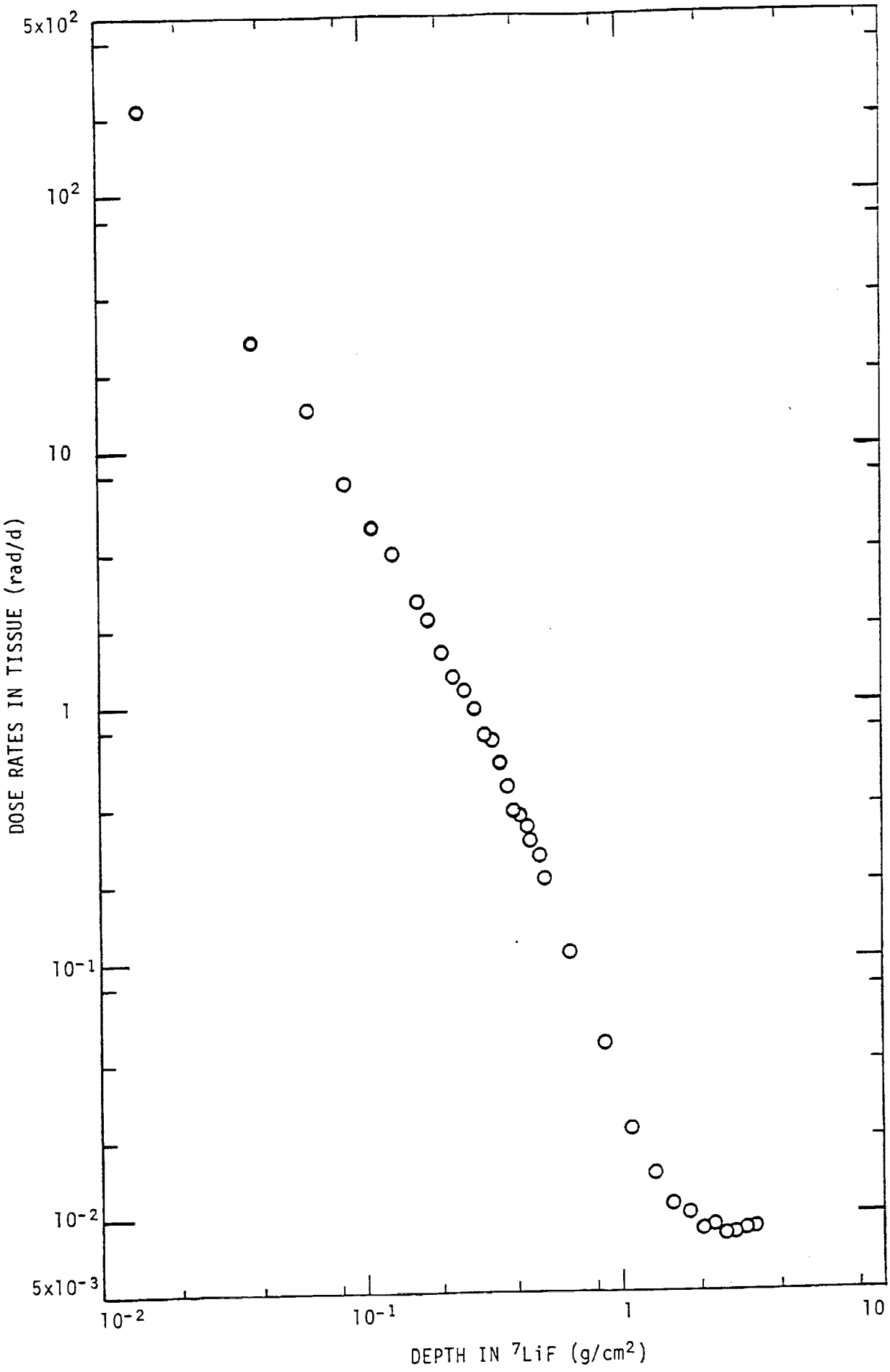

Fig. 12. Average dose rates in Plate No. B9-2 (TLD stacks Nos. 2, 6, 10)

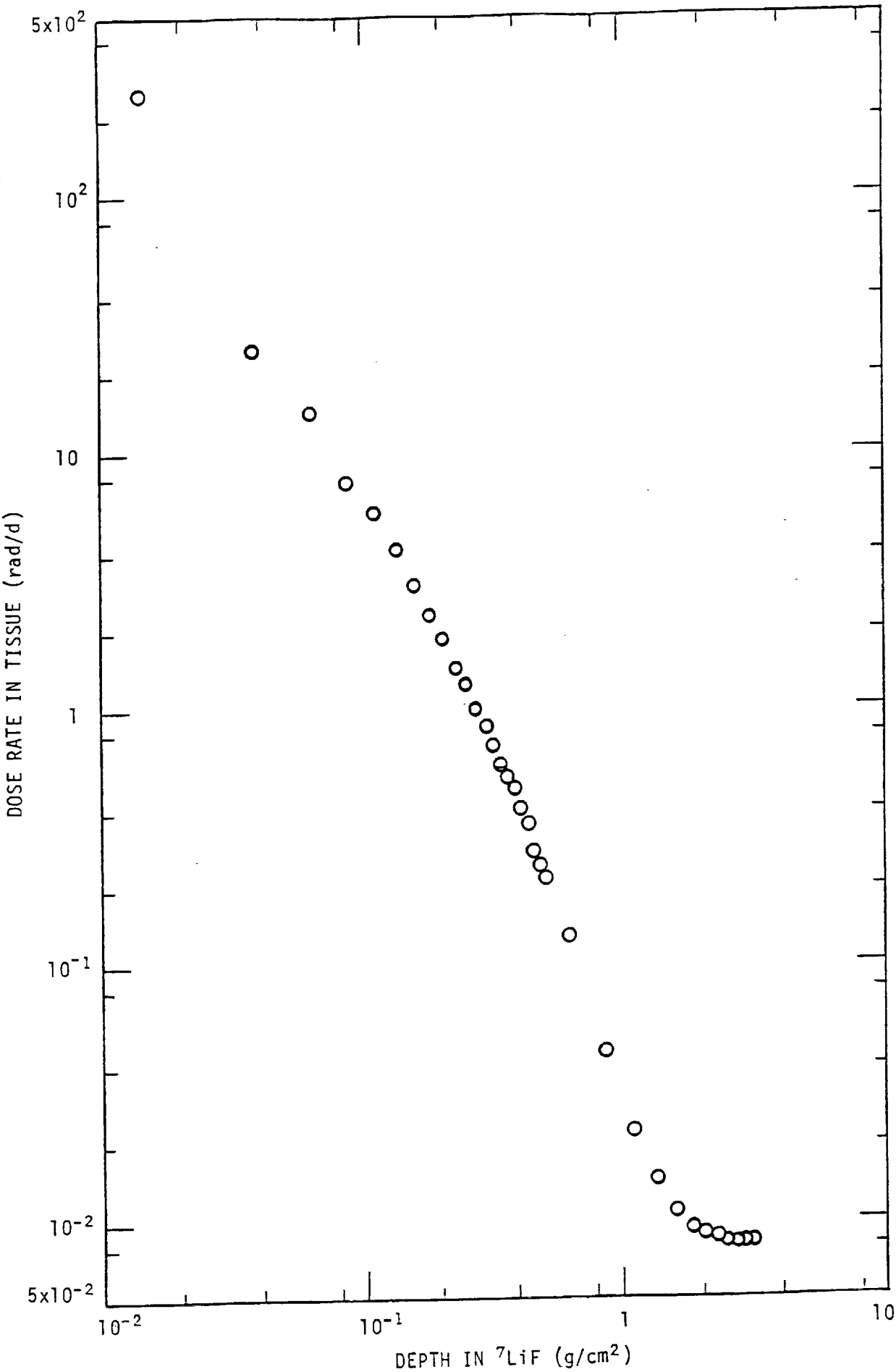

Fig. 13. Average dose rates in Plate No. B9-3 (TLD stacks Nos. 1, 3, 9)

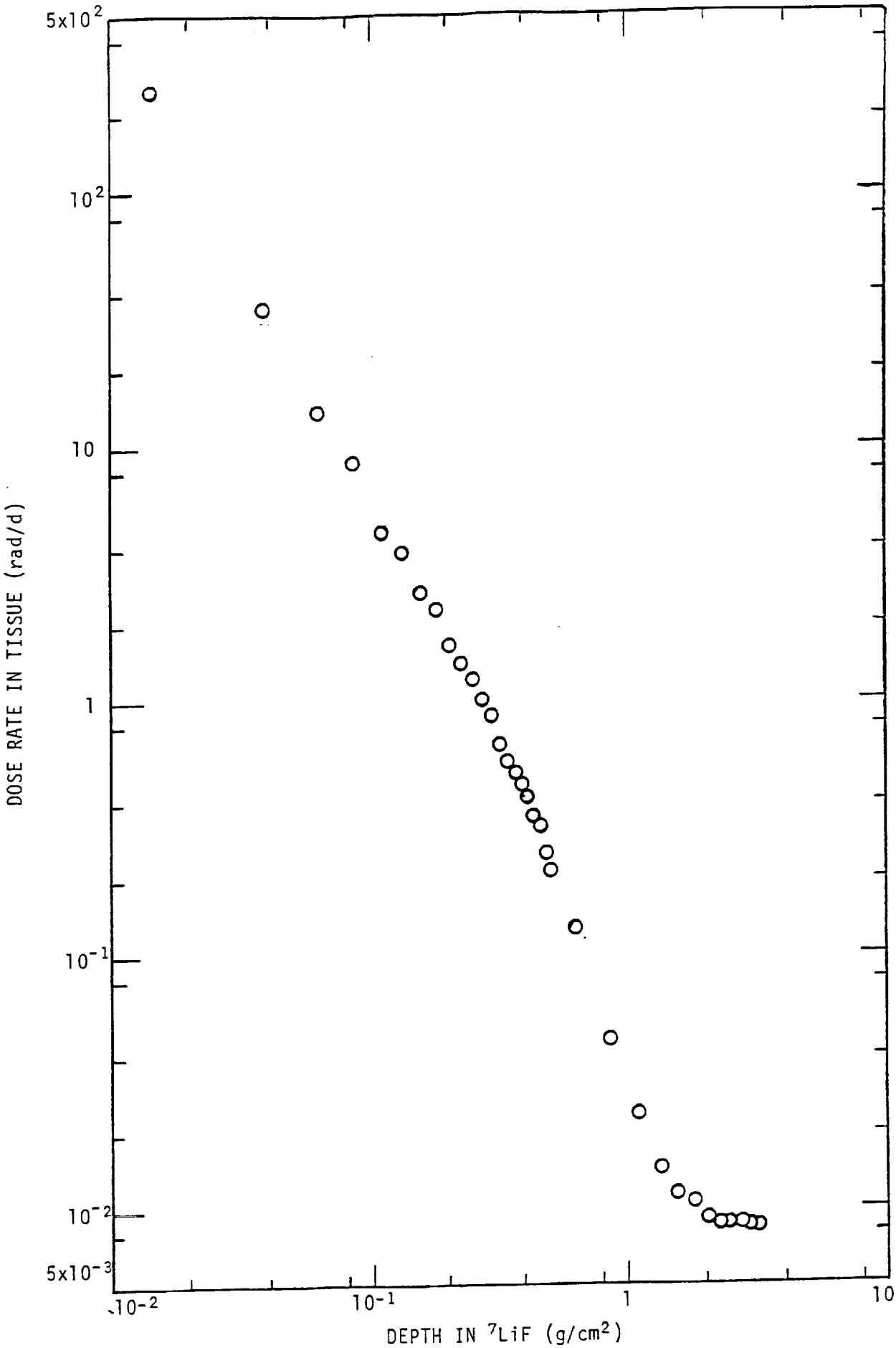

Fig. 14. Average dose rates in Plate No. B9-4 (TLD stacks Nos. 5, 7, 11)

TABLE 1 Cosmos 2044 Experiment K-7-41A TLD Stack Tissue Absorbed Dose Rates

Plate #B9-1 Ave.(rad/d)	Plate #B9-2 Ave.(rad/d)	Plate #B9-3 Ave.(rad/d)	Plate #B9-4 Ave.(rad/d)	Depth in ^{7}LiF (g/cm^2)
188	219	248	252	0.0146
22.1	27.0	24.9	35.0	0.0386
13.3	14.4	14.3	13.6	0.0625
7.32	7.39	7.54	8.55	0.0865
4.81	4.96	5.79	5.57	0.110
2.98	3.93	4.12	3.83	0.134
2.55	2.54	3.08	2.70	0.158
2.04	2.16	2.33	2.29	0.182
1.40	1.60	1.86	1.67	0.206
1.22	1.29	1.42	1.41	0.230
1.03	1.13	1.22	1.21	0.254
0.870	0.971	0.978	1.01	0.278
0.714	0.761	0.855	0.884	0.302
0.593	0.718	0.714	0.678	0.326
0.500	0.588	0.604	0.579	0.350
0.430	0.486	0.533	0.523	0.374
0.370	0.386	0.490	0.468	0.398
0.311	0.373	0.403	0.420	0.422
0.278	0.334	0.357	0.352	0.446
0.246	0.299	0.278	0.326	0.470
0.201	0.254	0.245	0.254	0.494
0.183	0.211	0.219	0.217	0.518
*				
0.0971	0.108	0.130	0.128	0.646
0.0380	0.0474	0.0457	0.0461	0.878
0.0204	0.0218	0.0225	0.0237	1.11
0.0135	0.0145	0.0145	0.0145	1.34
0.0115	0.0110	0.0108	0.0114	1.57
0.0104	0.0101	0.00928	0.0107	1.81
0.00971	0.00884	0.00899	0.00906	2.04
0.00978	0.00906	0.00862	0.00877	2.27
0.00949	0.00841	0.00841	0.00877	2.50
0.00913	0.00848	0.00826	0.00870	2.74
0.00942	0.00870	0.00833	0.00855	2.97
0.00935	0.00884	0.00848	0.00833	3.20

*Measurements from thicker TLDs below this point

TABLE 2a

COSMOS 2044 Experiment K-7-41A

TLD Stack Doses Plate No. B9-1

Stack No.4 (rad)	Stack No.8 (rad)	Stack No.12 (rad)	Plate No.B9-1 Average (rad)	Depth in ^{7}LiF (g/cm^2)
2080	2580	3130	2600	0.0146
285	362	268	305	0.0386
143	250	159	184	0.0625
95.6	112	94.3	101	0.0865
70.0	73.7	55.4	66.4	0.110
32.3	42.7	48.2	41.1	0.134
31.1	36.7	37.8	35.2	0.158
28.0	28.2	28.2	28.1	0.182
20.7	19.6	17.6	19.3	0.206
18.6	16.5	15.6	16.9	0.230
14.3	15.1	13.2	14.2	0.254
12.2	13.5	10.2	12.0	0.278
--	9.85	--	9.85	0.302
8.63	8.01	7.90	8.18	0.326
6.71	7.61	6.37	6.90	0.350
6.06	6.38	5.36	5.93	0.374
5.87	5.13	4.29	5.10	0.398
4.18	4.81	3.87	4.29	0.422
3.74	4.29	3.50	3.84	0.446
3.60	3.66	2.93	3.40	0.470
2.93	2.85	2.52	2.77	0.494
2.64	2.61	2.33	2.53	0.518
*				
1.32	1.42	1.27	1.34	0.646
0.511	0.556	0.507	0.525	0.878
0.275	0.289	0.281	0.282	1.11
0.184	0.201	0.174	0.186	1.34
0.159	0.167	0.150	0.159	1.57
0.145	0.137	0.148	0.143	1.81
0.131	0.137	0.135	0.134	2.04
0.129	0.140	0.136	0.135	2.27
0.126	0.135	0.132	0.131	2.50
0.122	0.127	0.128	0.126	2.74
0.133	0.121	0.136	0.130	2.97
--	0.134	0.124	0.129	3.20

*Measurements from thicker TLDs below this point

TABLE 2b

COSMOS 2044 Experiment K-7-41A

TLD Stack Doses Plate No. B9-2

Stack No.2 (rad)	Stack No.6 (rad)	Stack No.10 (rad)	Plate No.B9-2 Average (rad)	Depth in ^{7}LiF (g/cm^2)
2040	3410	3600	3020	0.0146
266	483	366	372	0.0386
131	232	235	199	0.0625
79.3	129	96.2	102	0.0865
62.3	79.4	63.7	68.5	0.110
44.1	73.2	45.7	54.3	0.134
27.9	46.6	30.7	35.1	0.158
31.6	33.0	24.7	29.8	0.182
19.7	27.3	19.2	22.1	0.206
15.8	21.4	16.3	17.8	0.230
14.0	21.1	11.8	15.6	0.254
11.4	18.0	10.7	13.4	0.278
9.78	13.3	8.33	10.5	0.302
9.65	11.2	8.89	9.91	0.326
8.35	9.31	6.66	8.11	0.350
6.59	8.15	5.40	6.71	0.374
5.04	6.35	4.58	5.32	0.398
5.27	5.89	4.28	5.15	0.422
4.49	5.33	4.01	4.61	0.446
4.35	4.80	3.24	4.13	0.470
3.38	4.21	2.92	3.50	0.494
2.85	3.67	2.22	2.91	0.518
*				
1.45	1.83	1.18	1.49	0.646
0.737	0.739	0.485	0.654	0.878
0.317	0.349	0.237	0.301	1.11
0.232	0.211	0.156	0.200	1.34
0.166	0.170	0.120	0.152	1.57
0.158	0.150	0.108	0.139	1.81
0.123	0.145	0.098	0.122	2.04
0.142	0.142	0.091	0.125	2.27
0.122	0.134	0.092	0.116	2.50
0.121	0.135	0.094	0.117	2.74
0.135	0.131	0.093	0.120	2.97
0.149	0.129	0.087	0.122	3.20

*Measurements from thicker TLDs below this point

TABLE 2c

COSMOS 2044 Experiment K-7-41A

TLD Stack Doses Plate No. B9-3

Stack No.1 (rad)	Stack No.3 (rad)	Stack No.9 (rad)	Plate No.B9-3 Average (rad)	Depth in ^{7}LiF (g/cm^2)
2380	3390	4480	3420	0.0146
295	343	390	343	0.0386
153	214	223	197	0.0625
89.8	113	110	104	0.0865
61.7	106	72.0	79.9	0.110
50.7	78.1	42.0	56.9	0.134
32.9	50.8	43.7	42.5	0.158
26.9	37.3	32.1	32.1	0.182
22.5	27.6	26.8	25.6	0.206
16.9	20.3	21.7	19.6	0.230
13.3	17.8	19.3	16.8	0.254
11.6	16.0	12.9	13.5	0.278
11.5	11.6	12.2	11.8	0.302
8.15	10.8	10.6	9.85	0.326
7.33	8.83	8.82	8.33	0.350
6.62	8.35	7.07	7.35	0.374
5.32	7.47	7.49	6.76	0.398
4.46	6.79	5.42	5.56	0.422
4.49	5.36	4.91	4.92	0.446
3.20	3.82	4.50	3.84	0.470
2.42	3.93	3.79	3.38	0.494
2.48	3.55	--	3.02	0.518
*				
1.56	2.01	1.82	1.80	0.646
0.479	0.729	0.683	0.630	0.878
0.237	0.346	0.349	0.311	1.11
0.144	0.227	0.228	0.200	1.34
0.105	0.174	0.167	0.149	1.57
0.097	0.152	0.134	0.128	1.81
0.085	0.140	0.147	0.124	2.04
0.089	0.135	0.133	0.119	2.27
0.086	0.133	0.128	0.116	2.50
0.079	0.128	0.134	0.114	2.74
0.084	0.129	0.133	0.115	2.97
0.091	0.127	0.133	0.117	3.20

*Measurements from thicker TLDs below this point

TABLE 2d

COSMOS 2044 Experiment K-7-41A

TLD Stack Doses Plate No. B9-4

Stack No.5 (rad)	Stack No.7 (rad)	Stack No.11 (rad)	Plate No.B9-4 Average (rad)	Depth in ^{7}LiF (g/cm^2)
2530	3750	4150	3480	0.0146
587	481	382	483	0.0386
167	196	202	188	0.0625
111	135	107	118	0.0865
64.7	83.4	82.3	76.8	0.110
48.6	52.1	58.0	52.9	0.134
34.1	40.8	37.1	37.3	0.158
28.4	34.5	32.0	31.6	0.182
20.5	23.9	24.5	23.0	0.206
18.0	18.5	21.6	19.4	0.230
14.4	15.3	20.5	16.7	0.254
12.9	13.4	15.3	13.9	0.278
10.9	12.4	13.2	12.2	0.302
9.18	9.51	--	9.35	0.326
7.96	8.01	--	7.99	0.350
6.34	7.40	7.91	7.22	0.374
5.58	6.86	6.93	6.46	0.398
4.83	6.41	6.13	5.79	0.422
4.62	5.43	4.53	4.86	0.446
4.82	4.25	4.43	4.50	0.470
3.07	3.75	3.67	3.50	0.494
2.87	2.84	3.25	2.99	0.518
*				
1.48	1.80	2.01	1.76	0.646
0.591	0.607	0.709	0.636	0.878
0.282	0.335	0.363	0.327	1.11
0.180	0.206	0.214	0.200	1.34
0.139	0.159	0.172	0.157	1.57
0.121	0.168	0.153	0.147	1.81
0.107	0.133	0.136	0.125	2.04
0.107	0.129	0.126	0.121	2.27
0.015	0.138	0.120	0.121	2.50
0.103	0.127	0.131	0.120	2.74
0.106	0.125	0.122	0.118	2.97
0.103	0.124	0.119	0.115	3.20

*Measurements from thicker TLDs below this point

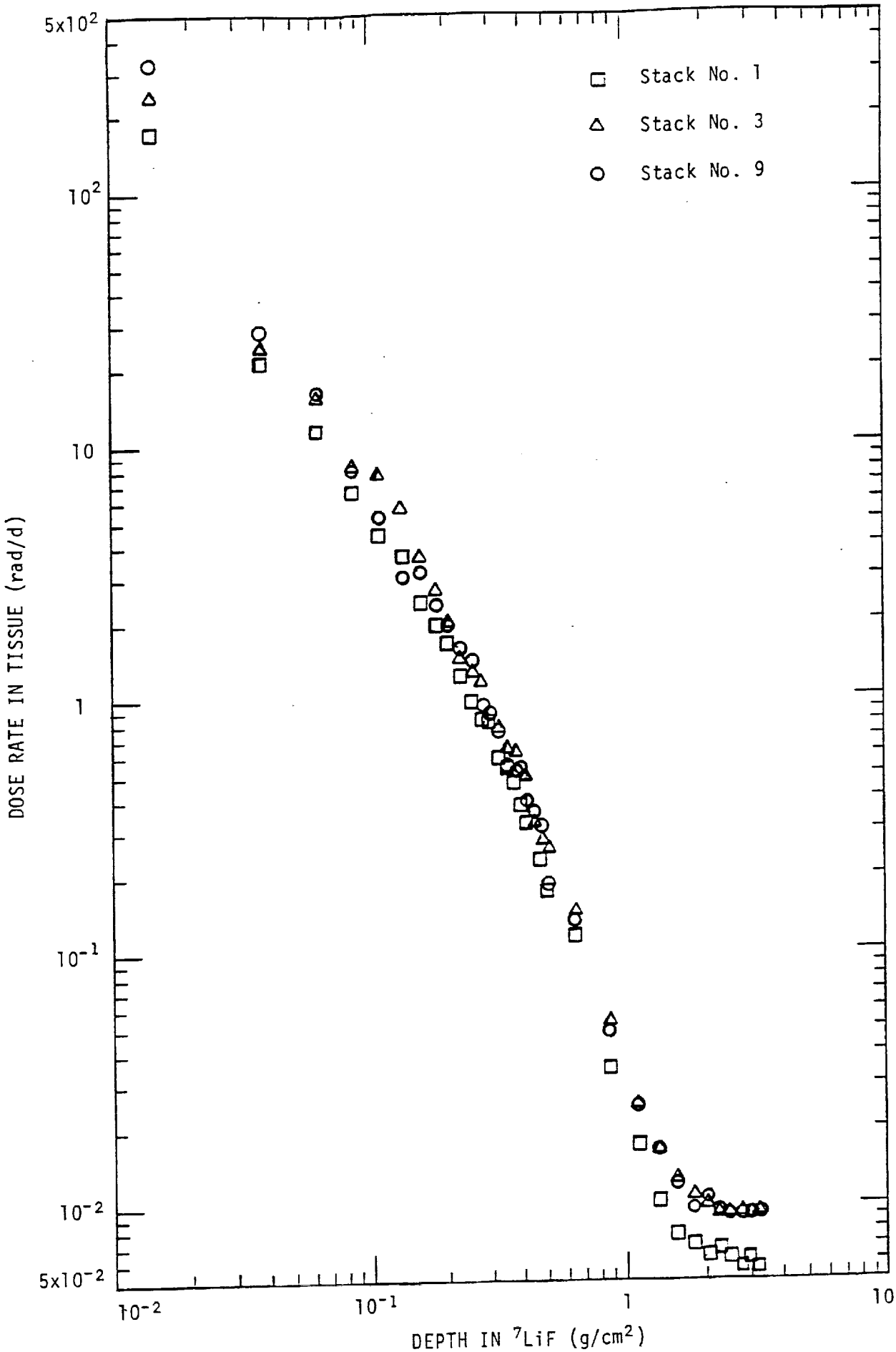

Fig. 15. Dose rates for the three TLD stacks in Plate No. B9-3

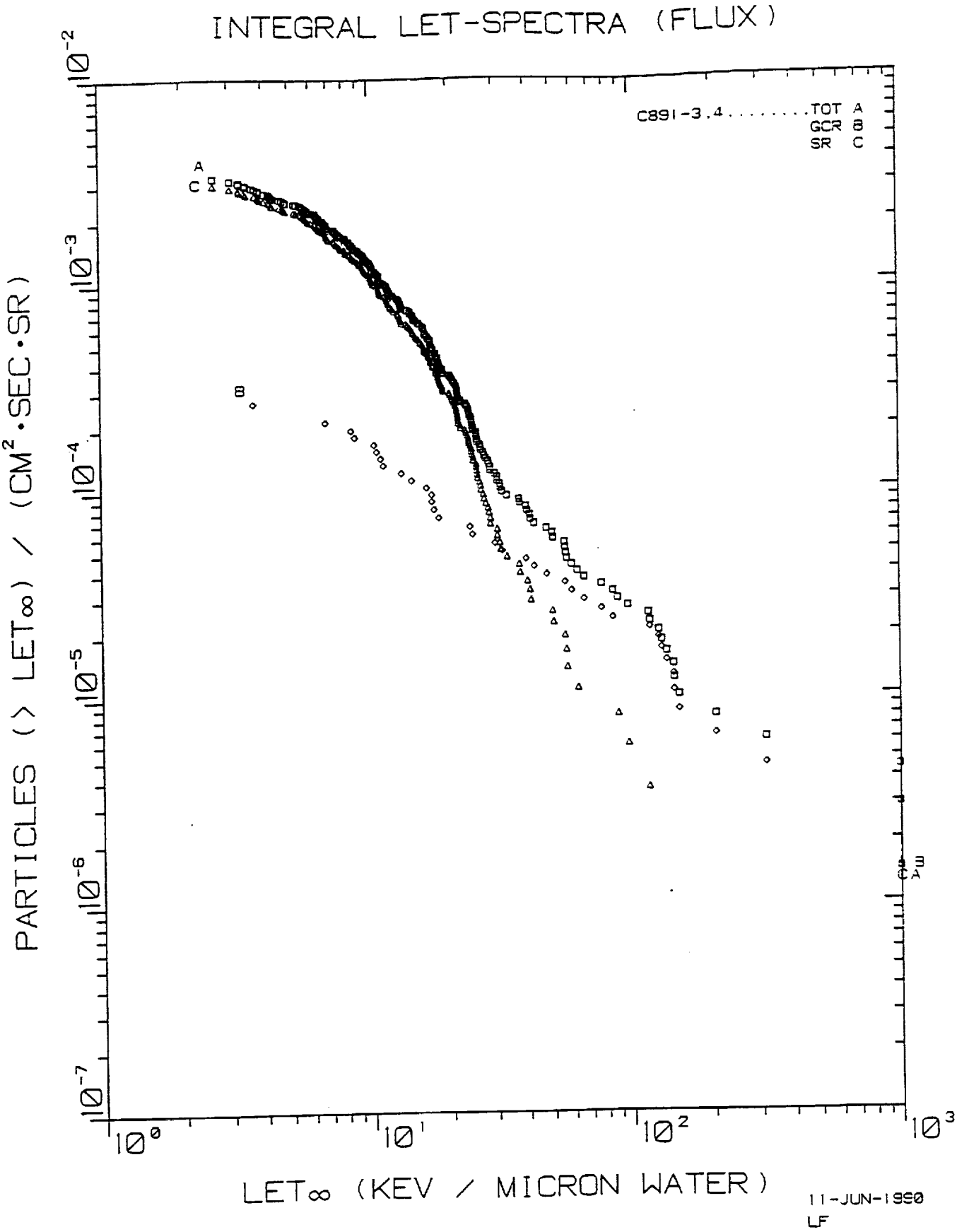

Fig. 16. Integral LET flux spectra for Experiment K-7-41B, PNTD stack F1 (outside the spacecraft). The minimum shielding was 0.164 g/cm^2 plastic.

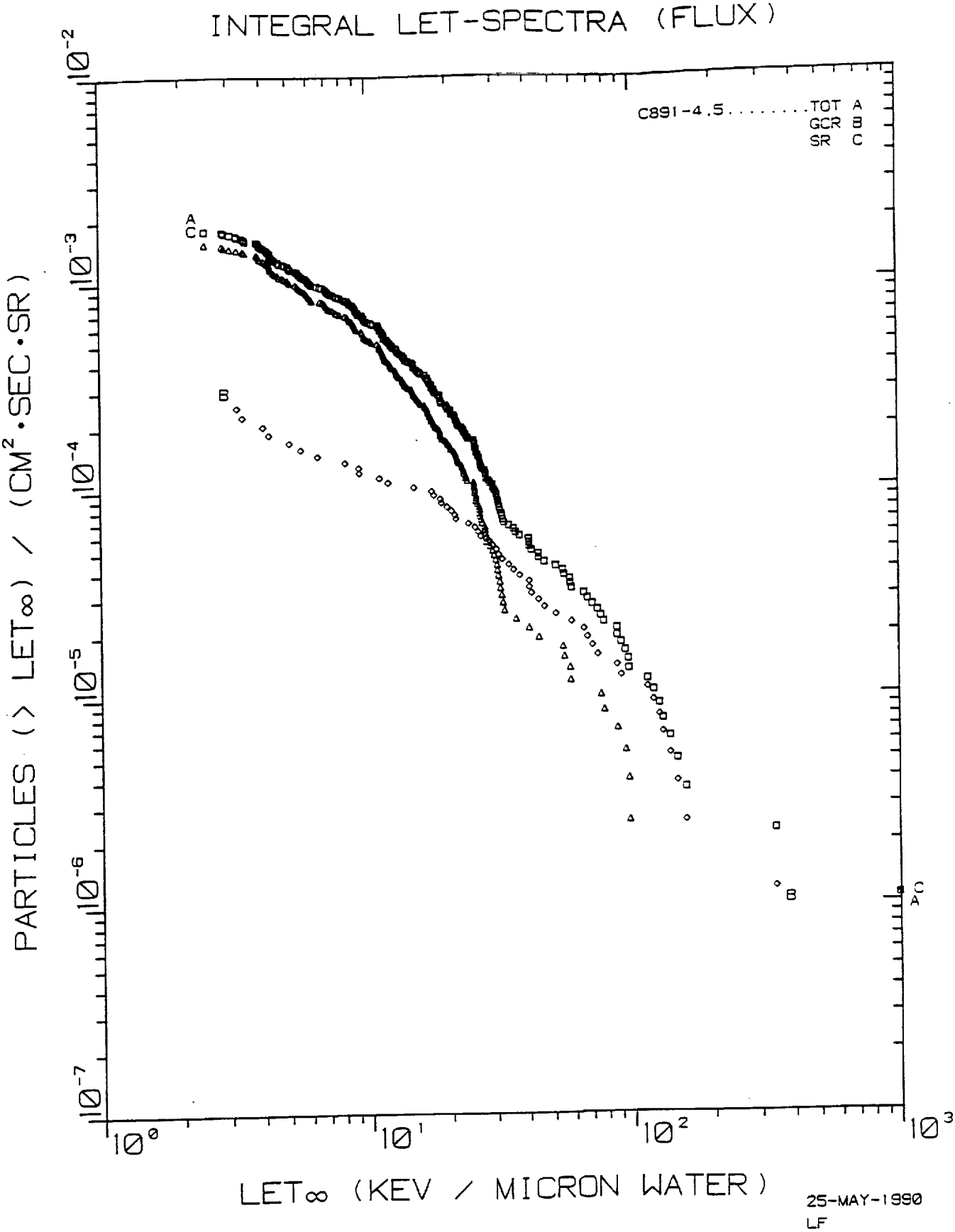

Fig. 17. Integral LET flux spectra for Exp. K-7-41B, PNTD stack F1 (outside the spacecraft). The minimum shielding was 0.239 g/cm^2 plastic.

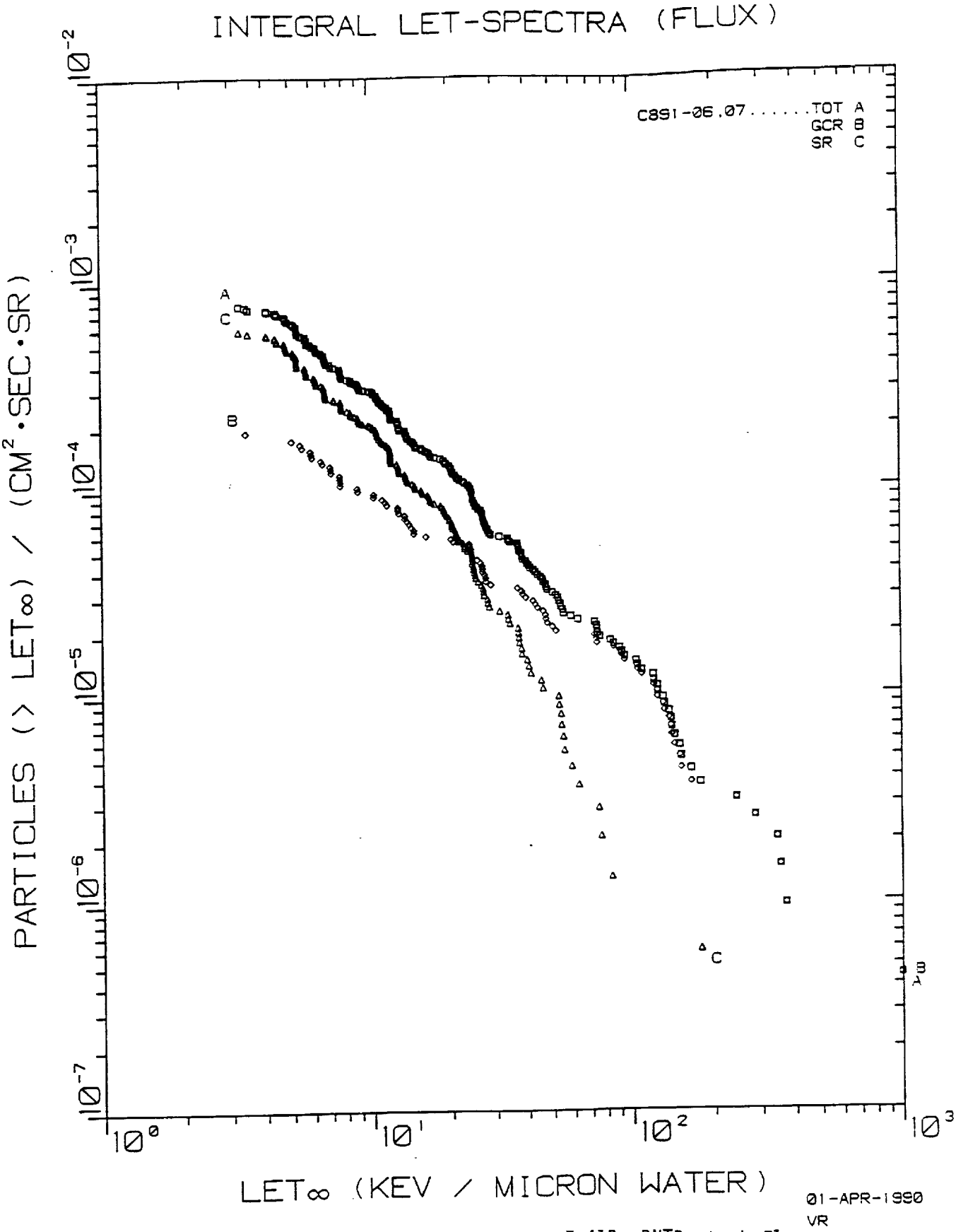

Fig. 18. Integral LET flux spectra for Exp. K-7-41B, PNTD stack F1 (outside the spacecraft). The minimum shielding was 0.397 g/cm^2 plastic.

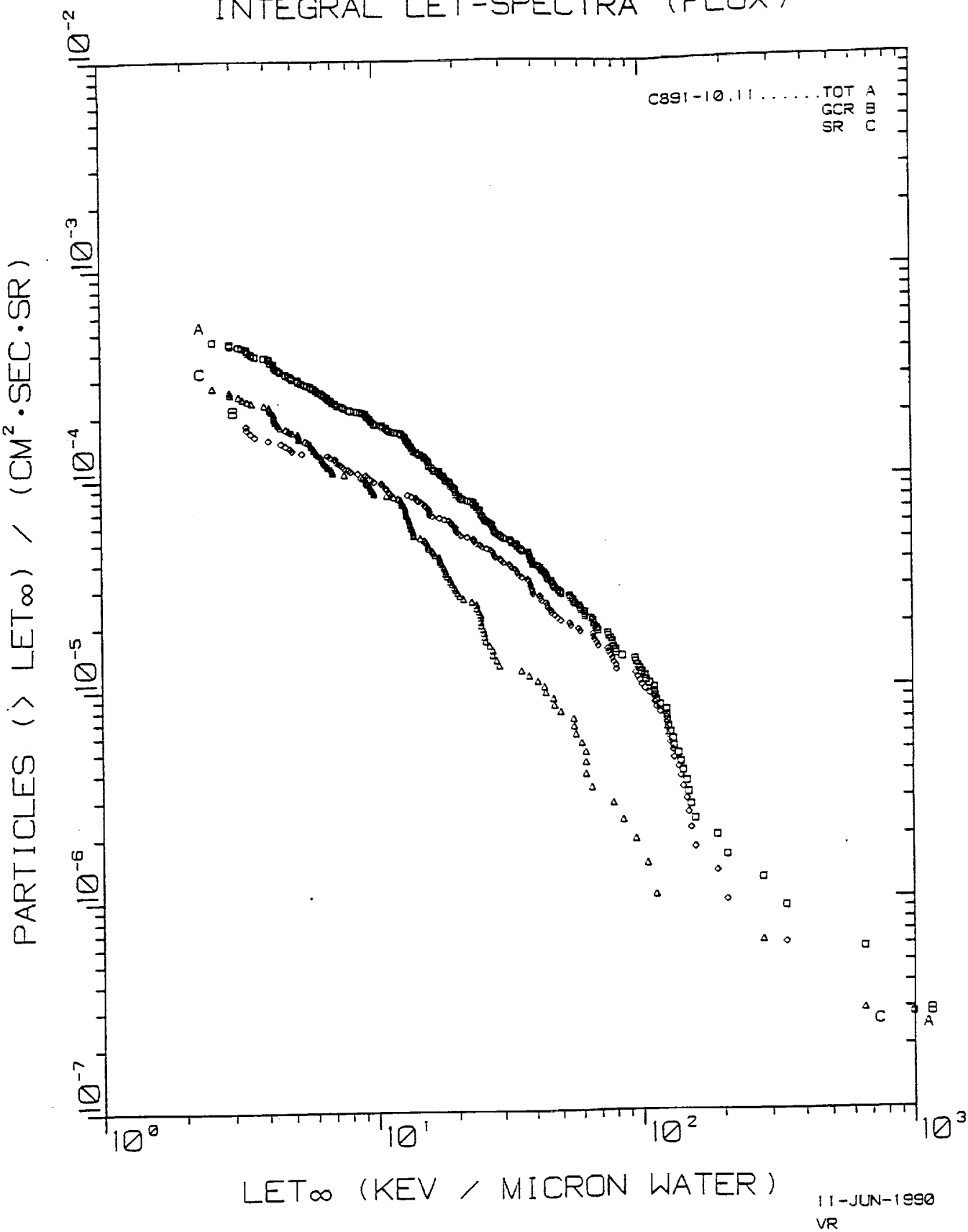

Fig. 19. Integral LET flux spectra for Exp. K-7-41B, PNTD stack F1 (outside the spacecraft). The minimum shielding was 1.47 g/cm^2 plastic, stainless steel and nuclear emulsion.

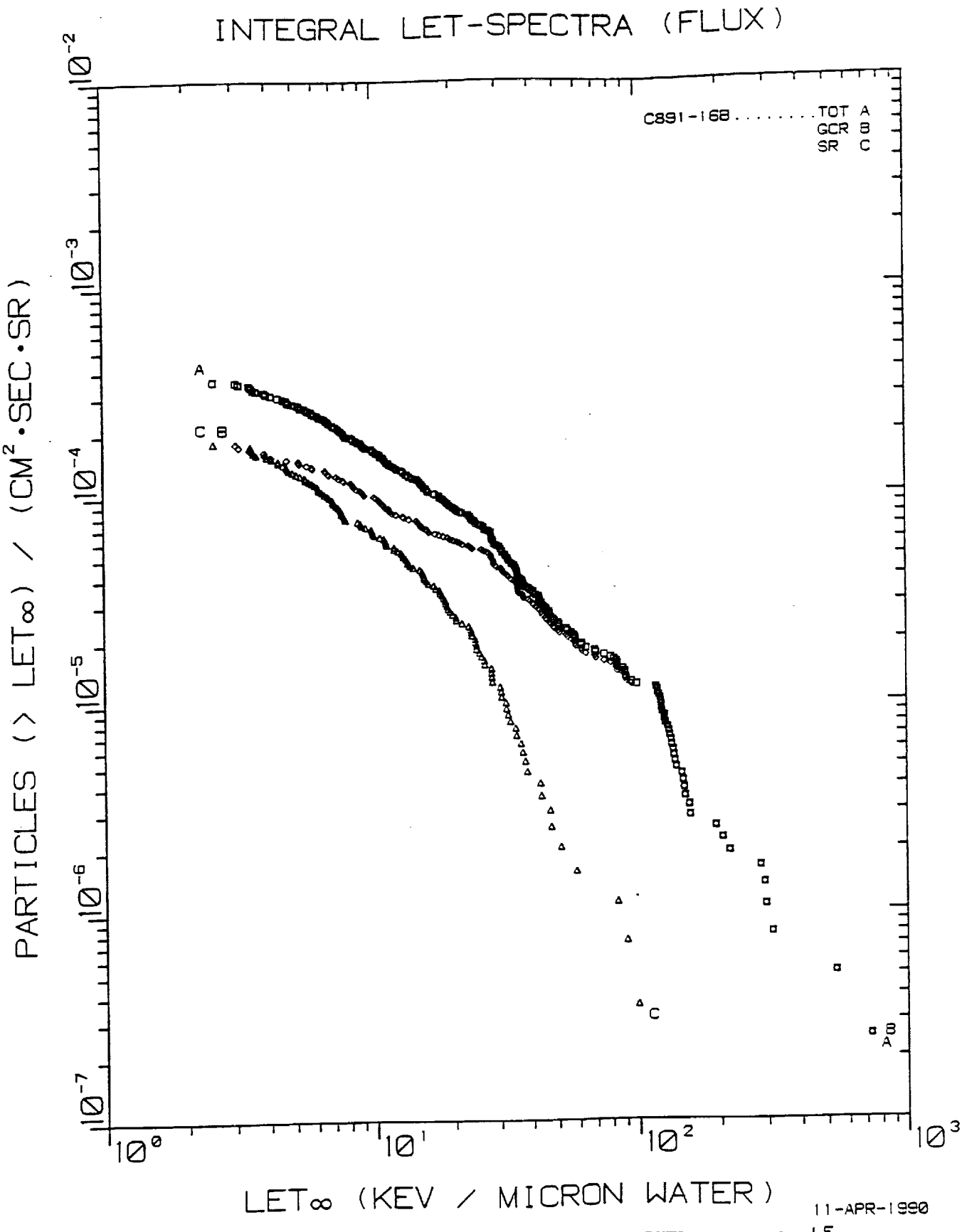

Fig. 20. Integral LET flux spectra for Exp. K-7-41B, PNTD stack F1 (outside the spacecraft). The minimum shielding was 1.95 g/cm^2 plastic, stainless steel and nuclear emulsion.

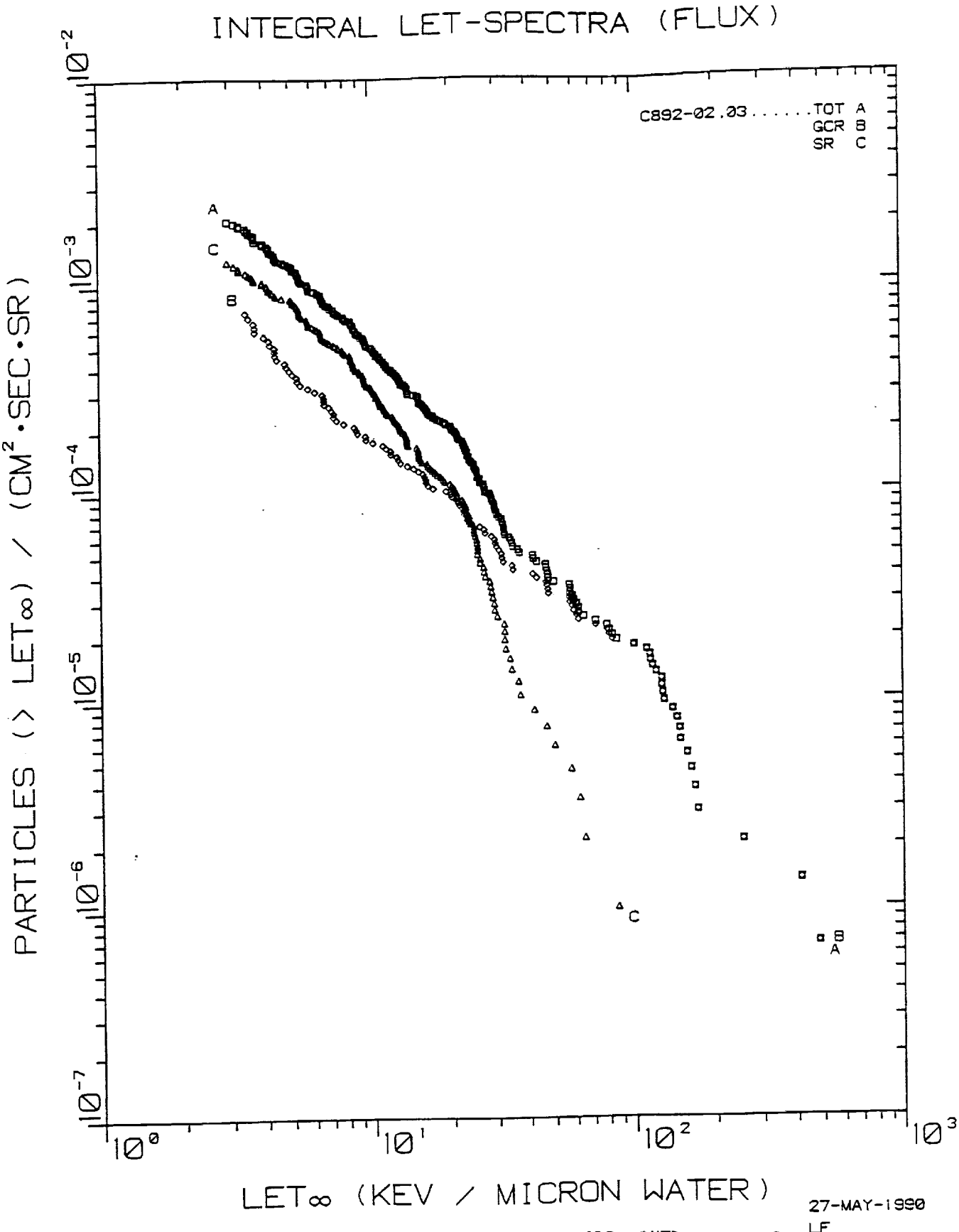

Fig. 21. Integral LET flux spectra for Exp. K-7-41B, PNTD Stack F2 (outside the spacecraft). The minimum shielding was 0.0935 g/cm^2 plastic.

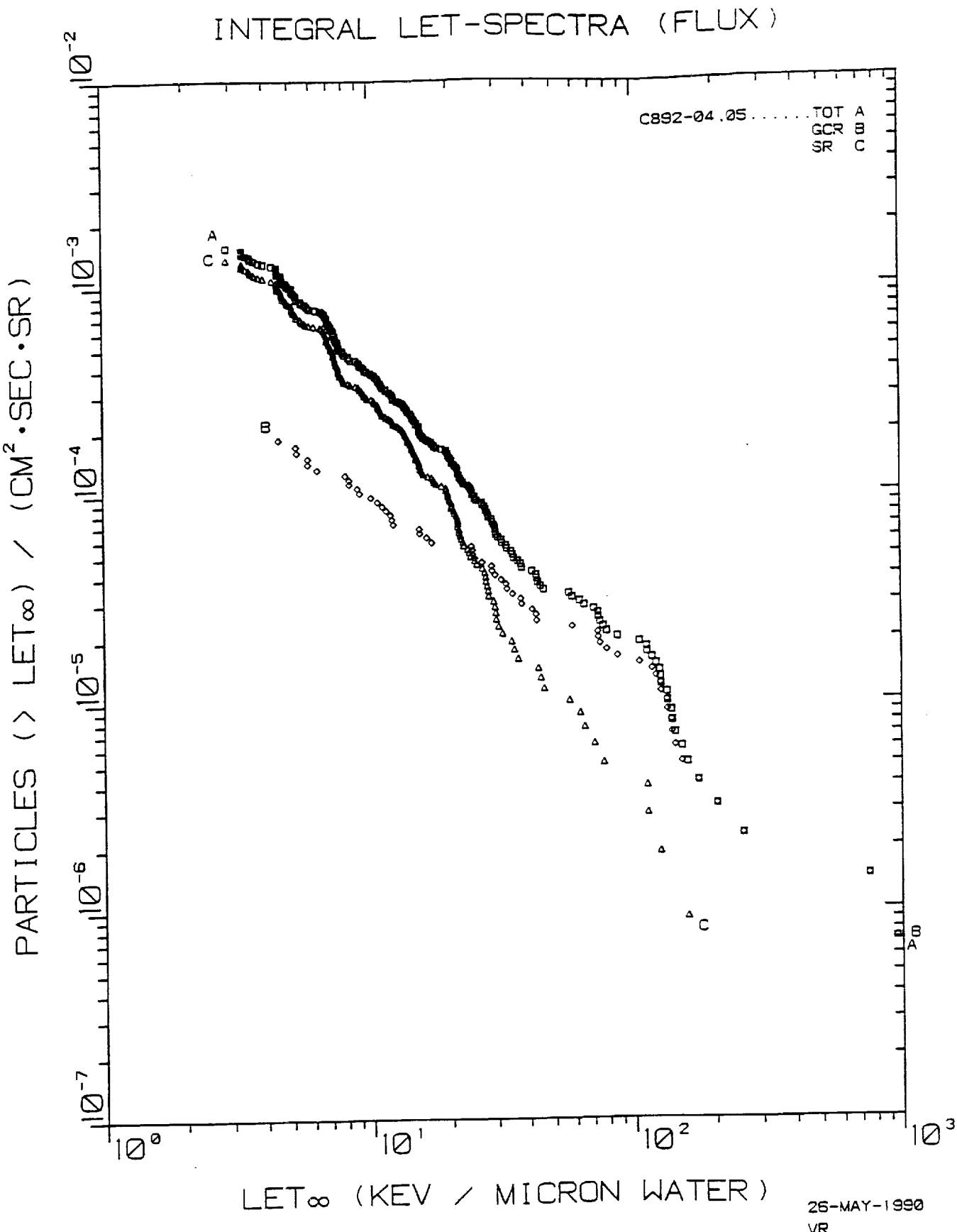

Fig. 22. Integral LET flux spectra for Exp. K-7-41B, PNTD stack F2 (outside the spacecraft). The minimum shielding was 0.250 g/cm^2 plastic.

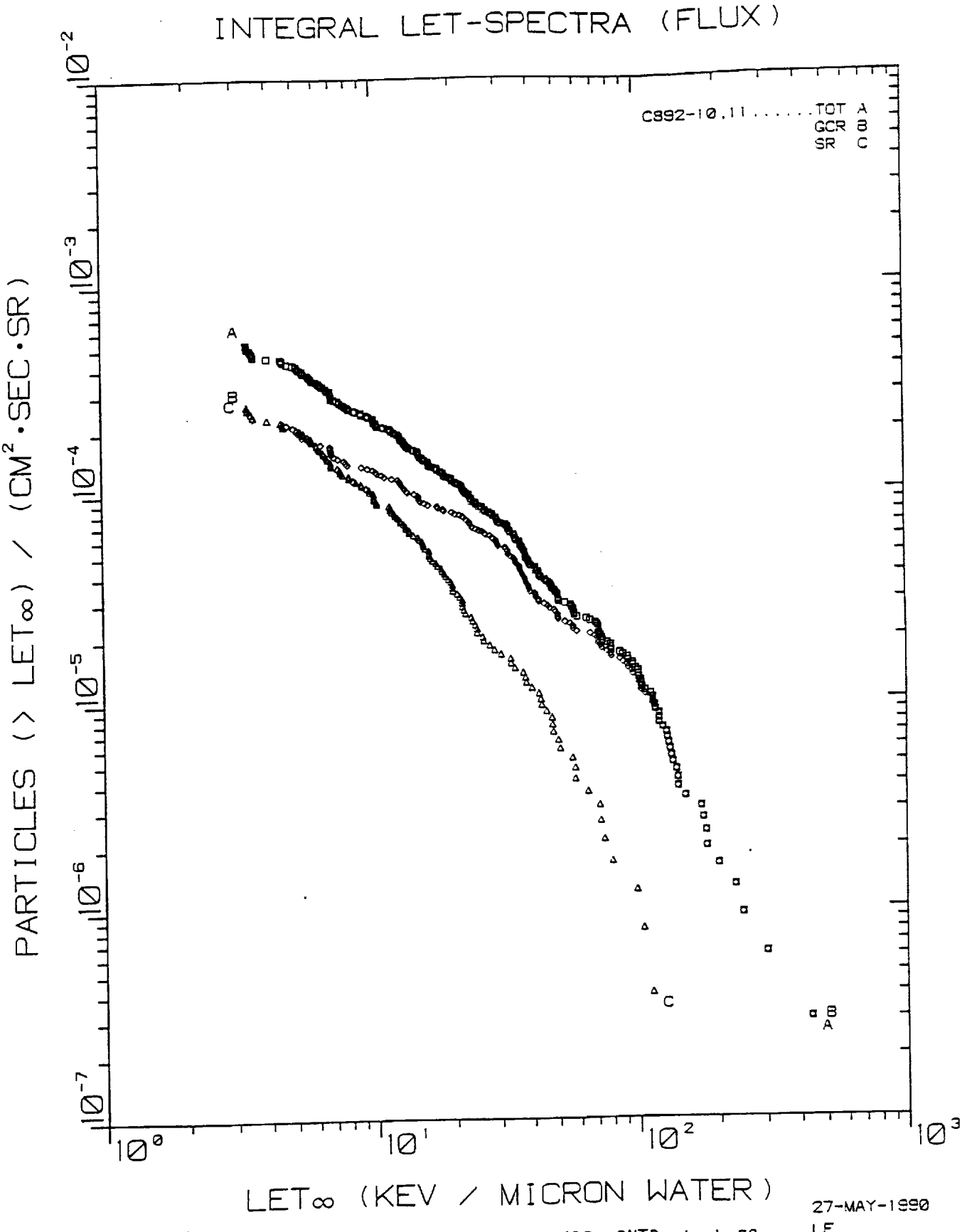

Fig. 23. Integral LET flux spectra for Exp. K-7-41B, PNTD stack F2 (outside the spacecraft). The minimum shielding was 1.49 g/cm^2 plastic, stainless steel and nuclear emulsion.

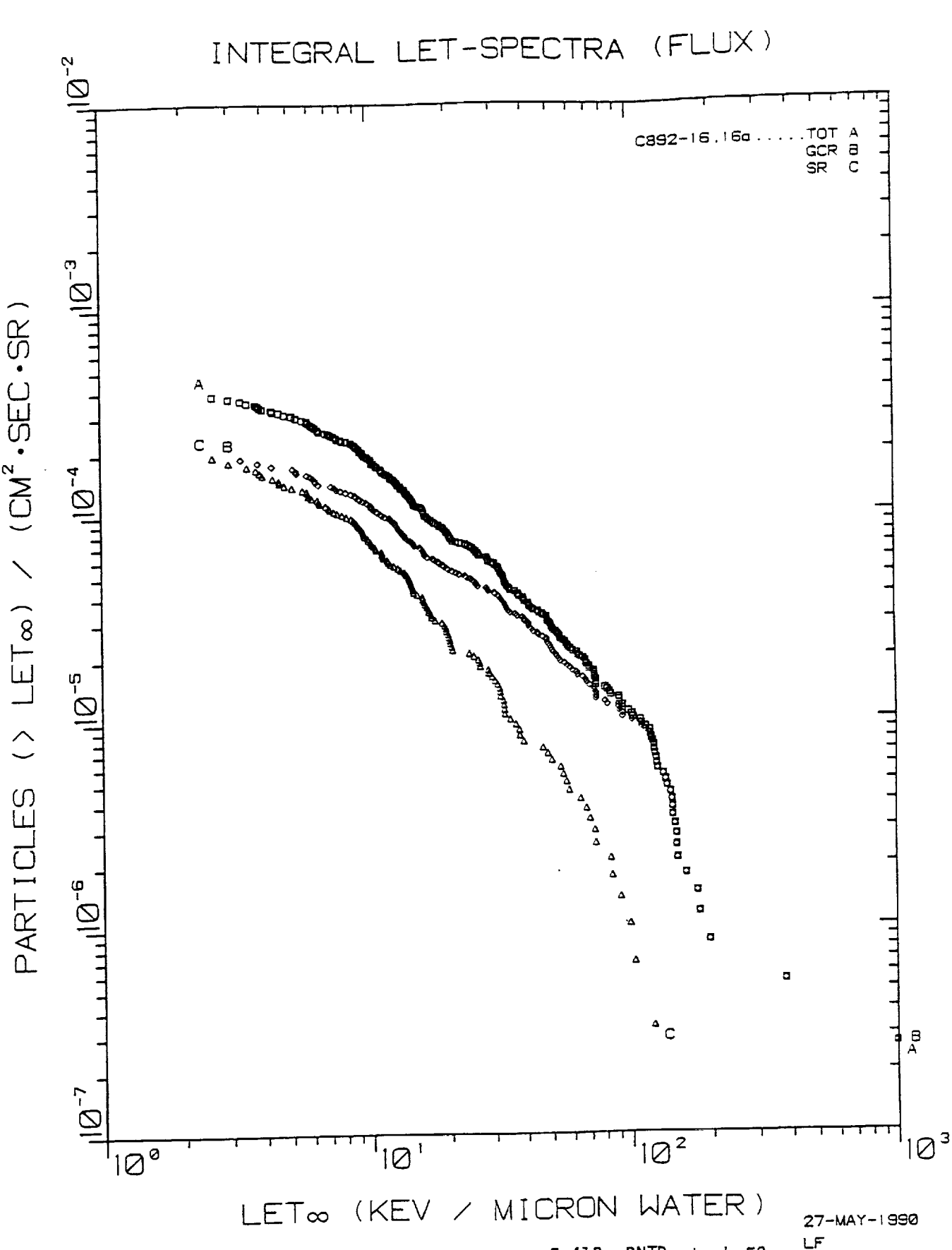

Fig. 24. Integral LET flux spectra for Exp. K-7-41B, PNTD stack F2 (outside the spacecraft). The minimum shielding was 1.97 g/cm² plastic, stainless steel and nuclear emulsion.

The decrease in total flux with increasing shielding thickness is obvious in both F1 and F2. However, the least shielded PNTD in F1 has a greater integral flux than that in F2 (factor of 1.7) despite being more heavily shielded. This demonstrates a directional dependence of incoming radiation with F1 (Plate B9-2 in Container KHA-1) being in better alignment with the direction of maximum flux than F2 (Plate B9-1 in Container KHA-3).

The integral measurements are given numerically in Tables 3a and 3b. The differences between F1 and F2 are seen to be greatest at small shielding thicknesses. A comparison of fluxes, dose rates and dose equivalent rates reveals that average particle LET increases with shielding thickness (dose rate/flux and dose equivalent rate/dose rate increase as average LET increases). This agrees with previous measurements on Cosmos 1887. The fraction of total flux due to SR particles decreases with shielding thickness, although this is irregular in F2. The above two observances are consistent with a more rapid filtering out of low energy protons than of higher Z particles with increasing shielding.

The nuclear emulsions which were a part of the detector stacks are still undergoing analysis and will be reported at a later time.

Part C

The ^{59}Co activation foils have been read out. Background studies and data analysis are still in progress. The results will be reported at a later time.

Part D

The measurement results from the ^{232}Th/mica fission foil detectors are given in Table 4. Each flight detector included eight mica discs (0.5 in diameter). The statistical standard deviations of the measurements were computed from the scatter of the eight counted track densities. There is a 15% difference between the neutron fluxes for the two flight units but this difference is within the limits of accuracy of the track counting statistics. The average dose equivalent rate of high energy neutrons for the mission was 3.3 mrem/d.

Part E

The results of the ^{6}LiF/CR-39 thermal and resonance neutron measurements are given in Table 5. An obvious feature is the much smaller resonance neutron dose in detector F1 as compared to F2. The CR-39 detectors both

TABLE 3a PNTD Results From K-7-41B*

Detector	Min. Shielding (g/cm^2)	Spectrum Type	Flux ($cm^{-2} \cdot s^{-1} \cdot sr^{-1}$) $\times 10^{-4}$	Dose Rate (mrad/d)	Dose Equiv. Rate (mrem/d)
F1	0.164	TOT	27.29	7.01	53.8
		GCR	2.11	1.66	23.9
		SR	25.18	5.35	29.9
	0.239	TOT	14.85	3.72	27.2
		GCR	2.02	0.94	10.1
		SR	12.83	2.78	17.1
	0.397	TOT	7.30	2.03	17.8
		GCR	1.72	0.94	12.0
		SR	5.58	1.09	5.8
	1.47	TOT	3.73	1.32	12.8
		GCR	1.52	0.79	9.0
		SR	2.21	0.53	3.8
	1.95	TOT	3.05	1.20	12.3
		GCR	1.52	0.86	10.3
		SR	1.53	0.34	2.0

*For $LET_{\infty} \cdot H_2O \geq 4$ keV/μm

Note: For the three least-shielded detectors the shielding materials were plastic. For the two detectors with greater shielding, the shielding material included 0.591 g/cm^2 of stainless steel and 0.120 g/cm^2 of nuclear emulsion.

TABLE 3b PNTD Results From K-7-41B*

Detector	Min. Shielding (g/cm^2)	Spectrum Type	Flux ($cm^{-2} \cdot s^{-1} \cdot sr^{-1}$) $\times 10^{-4}$	Dose Rate (mrad/d)	Dose Equiv.Rate (mrem/d)
F2	0.0935	TOT	15.83	3.35	23.3
		GCR	5.60	1.56	15.2
		SR	10.23	1.79	8.1
	0.250	TOT	12.74	2.89	22.9
		GCR	1.82	1.03	13.7
		SR	10.92	1.86	9.2
	1.49	TOT	4.47	1.53	13.9
		GCR	2.20	1.00	10.7
		SR	2.27	0.53	3.2
	1.97	TOT	3.27	1.22	11.6
		GCR	1.72	0.82	9.0
		SR	1.55	0.40	2.6

*For $LET_{\infty} \cdot H_2O \geq 4$ keV/μm

Note: For the two least shielded detectors the shielding materials were plastic. For the two detectors with greater shielding, the shielding material included 0.591 g/cm^2 of stainless steel and 0.120 g/cm^2 of nuclear emulsion.

TABLE 4

Experiment K-7-41D: High Energy Neutron Measurements with ^{232}Th/mica Detectors

Flight Detector	Neutron Fluence (cm^{-2})	Neutron Flux ($cm^{-2}d^{-1}$)	Dose Equiv. (mrem)	Dose Equiv. Rate (mrem d^{-1})
F1	$8.1\pm1.1\times10^{5}$	$5.9\pm0.8\times10^{4}$	48±7	3.5±0.5
F2	$7.0\pm1.1\times10^{5}$	$5.1\pm0.8\times10^{4}$	42±7	3.0±0.5

*Measurements are for neutron energies > 1 MeV

Note: The standard deviations of the measurements are those due to counting statistics only. The absolute accuracy is uncertain because of assumptions of neutron and proton spectral shapes and the ratio between neutron and proton fluxes which are used in the data reduction. The probable accuracy of the numbers is within a factor of 3.

TABLE 5

Experiment K-7-41E: Thermal and Resonance Neutron Measurements

Detector	Energy Range	Neutron / cm^2	Dose Equiv. (mrem)	Dose Equiv.Rate (mrem/d)
F1	≤0.2eV	$2.56\pm0.16\times10^{5}$	0.26±0.02	0.019±0.002
	0.2eV<E_n<1MeV	$0.99\pm1.16\times10^{5}$	0.49±0.59	0.036±0.041
F2	≤0.2eV	$2.23\pm0.16\times10^{5}$	0.23±0.02	0.017±0.002
	0.2eV<E_n<1MeV	$6.8\pm1.3\times10^{5}$	3.4 ±0.6	0.25 ±0.04
GC	≤0.2eV	$0.15\pm0.05\times10^{5}$	0.02±0.01	
	0.2eV<E_n<1MeV	$4.29\pm0.46\times10^{5}$	2.1 ±0.2	

Note: The standard deviations of the measurements are those due to counting statistics only. Probable accuracy is +/- 20% for thermal neutrons and a factor of 2 for resonance neutrons.

above (space side) and below (spacecraft side) the ^{6}LiF layer confirmed the difference. Most of the tracks measured in F2 were on the space side of the ^{6}LiF layer. The space side CR-39 yielded a track density 2.7 times higher than the spacecraft side CR-39. This could imply a large epithermal neutron flux, incident from the space side of detector F2, which was not present in detector F1. However, as mentioned in the Readout section, the background subtraction from the detectors contained an element of uncertainty. It is possible that the experimental uncertainty in the resonance neutron results is larger than expected. Because of the method of subtraction in the data reduction, the thermal neutron results are much less affected than the resonance results.

SUMMARY AND DISCUSSION

The results from Cosmos 2044 are compared with previous Cosmos measurements in Table 6. It is seen in the TLD results that in the total absorbed dose rates for tissue found outside the spacecraft there is a greater spread on Cosmos 2044 when compared to Cosmos 1887. The maximum dose rate (minimum shielding) is greater and the minimum dose rate (maximum shielding) is less. This indicates that the higher inclination, lower altitude orbit of 2044 must have encountered greater trapped electron fluxes but smaller trapped proton fluxes than 1887. The smaller trapped proton fluxes can be explained in that the lower altitude Cosmos 2044 orbit passed beneath the higher flux region in the South Atlantic Anomaly (SAA). The greater trapped electron fluxes are due to the extension of the electron belt horns to lower altitudes at the higher latitudes. The large uncertainties seen in the maximum and minimum dose rates on Cosmos 2044 are due to the spread in the three measurements of the TLD stacks in Plate No. B9-4.

The PNTD measurements on Cosmos 2044 are directly comparable with those of Cosmos 1887 outside the spacecraft. It can be seen that while the maximum flux on 2044 is 0.80 times as high as on 1887, the dose equivalent rate is 1.75 times higher. The average LET, and also particle Z, were greater on Cosmos 2044. This is consistent with the higher inclination, lower altitude orbit and the resulting greater relative contribution from GCRs.

The thermal and resonance neutron fluxes and dose equivalent rates were less than previously measured, but on Cosmos 2044 the measurements were

TABLE 6. RADIATION MEASUREMENTS ON JOINT US/USSR COSMOS FLIGHTS

FLIGHT NO.	782	936	1129	1887	2044
Launch Date	Nov. 1975	Aug. 1977	Sept. 1979	Sept. 1987	Sept. 1989
Duration (d)	19.50	18.50	18.56	12.63	13.80
Inclination (°)	62.8	62.8	62.8	62.8	82.3
Altitude (km)-- Apogee/Perigee	405/226	419/224	394/226	406/224	294/216
TLD DOSE RATE					
Outside (max) (mrad d^{-1})				$1.78\pm0.19\times10^{5}$	$2.52\pm0.50\times10^{5}$
Outside (min) (mrad d^{-1})				28.0 ± 1.4	8.3 ± 0.6
Inside (mrad d^{-1})		25.6 ± 1.3	$18.0\pm3.6^{\dagger\dagger}$	24.8 ± 1.0	
HEAVY PARTICLES					
Flux Inside ($cm^{-2}s^{-1}sr^{-1}$)	$8.7\pm1.4\times10^{-6}$*	$5.1\pm1.0\times10^{-6}{}^{\Delta}$	$6.1\pm0.1\times10^{-7}{}^{\nabla}$	$4.25\pm0.24\times10^{-4}{}^{\dagger}$	
Flux Outside ($cm^{-2}s^{-1}sr^{-1}$)			$1.21\pm0.02\times10^{-6}{}^{\nabla}$	$3.43\pm0.22\times10^{-3}{}^{\dagger}$	$2.73\pm0.17\times10^{-3}{}^{\dagger}$
Dose Equivalent Rate Inside (mrem d^{-1})				11.4 ± 0.7	
Outside (mrem d^{-1})				30.8 ± 2.0	53.8 ± 3.6
NEUTRONS					
Thermal Flux (cm^{-2} d^{-1})		$1.9\pm0.4\times10^{4}$	$2.7\pm0.5\times10^{4}$		$1.7\pm0.4\times10^{4}$
Resonance Flux (cm^{-2} d^{-1})		$6.5\pm3.2\times10^{4}$	$7.5\pm3.8\times10^{4}$		$5.0\pm2.5\times10^{4}$
High Energy Flux (cm^{-2} d^{-1})		$1.1\pm---\times10^{5}$	$1.1\pm---\times10^{5}$		$5.5\pm---\times10^{4}$
Thermal Dose (mrem d^{-1})		0.020 ± 0.004	0.028 ± 0.006		0.018 ± 0.004
Resonance Dose (mrem d^{-1})		0.32 ± 0.16	0.40 ± 0.20		0.25 ± 0.13
High Energy Dose (mrem d^{-1})		$6.8\pm?$	$6.8\pm?$		$3.3\pm?$

*$LET_{\infty}\cdot H_2O \geq 105$ keV μm^{-1}; >100 μm range. $^{\Delta}LET_{\infty}\cdot H_2O \geq 106$ keV μm^{-1}; >180 μm range.
$^{\nabla}$Different processing; results not comparable to other flights.
$^{\dagger}LET_{\infty}\cdot H_2O \geq 4$ keV μm^{-1}; >100 μm range. ††Detectors irradiated during return transportation

on the outside of the spacecraft, while previous measurements were inside. Their comparability is therefore questionable.

The high energy neutrons have about half the flux and dose rate measured on Cosmos 936 and 1129; however, this comparison is also between detectors outside and inside the spacecraft.

In Figure 25, a measured depth dose profile in TLD-700 is compared with calculated depth doses for trapped electrons and protons behind plane aluminum shields for the Cosmos 2044 orbit at solar maximum /Watts, 1990/. This demonstrates that for shielding thicknesses up to 1 g/cm^2 trapped electrons contribute most of the dose. The model electron spectrum appears deficient at very low energies and somewhat harder than that measured. The trapped proton dose rate drops to about 0.001 rad/d at 3 g/cm^2, where the electron dose is a very small fraction of the total. This is a factor of 8 lower than the measurements. GCRs dominate total doses under thicker shielding for the Cosmos 2044 orbit, so this general result is expected.

In Figures 26 and 27, measured LET spectra under 0.0935 g/cm^2 are plotted with some recent calculations made with the NRL CREME code. In Figure 26, an SR spectrum is compared with calculations which omit GCRs with $Z > 2$. Most of the contributions to short-range tracks are included in these calculations. The fit below 100 MeV-cm^2/g (10 keV/μm) begins to diverge, but, as discussed above, the experimental measurements can also diverge in this LET region due to directional effects. The calculations are averaged over angle of incidence.

In Figure 27, the total flux spectrum is compared with calculations which include the GCRs through Z=28 (the contribution from particles with $Z > 28$ is insignificant). The measured spectrum falls somewhat below the spectrum for the nearest calculated shielding (0.1 g/cm^2). It should be noted that there is some loss from the measured spectrum due to loss of very short tracks in etching of the PNTDs. However, the agreement between measurements and calculations may be off by a factor of 2 because of basic difficulties in modeling the orbital radiation environment.

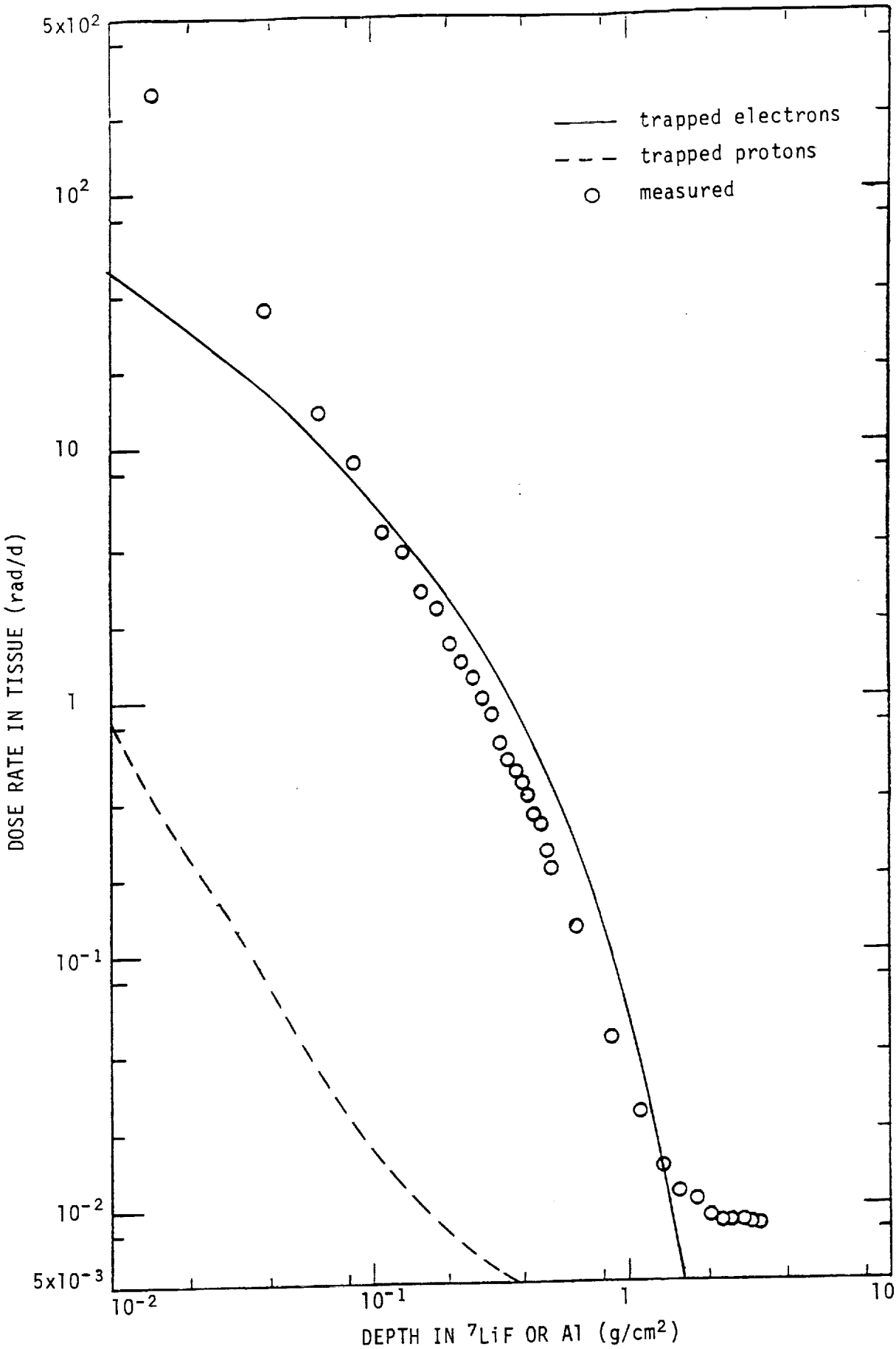

Fig. 25. Comparison of the average TLD dose rates in Plate No. B9-4 with the calculated depth dose rates of trapped electrons and protons for tissue behind aluminum plane shields /Watts, 1990/. The calculations were for the Cosmos 2044 orbit at solar maximum.

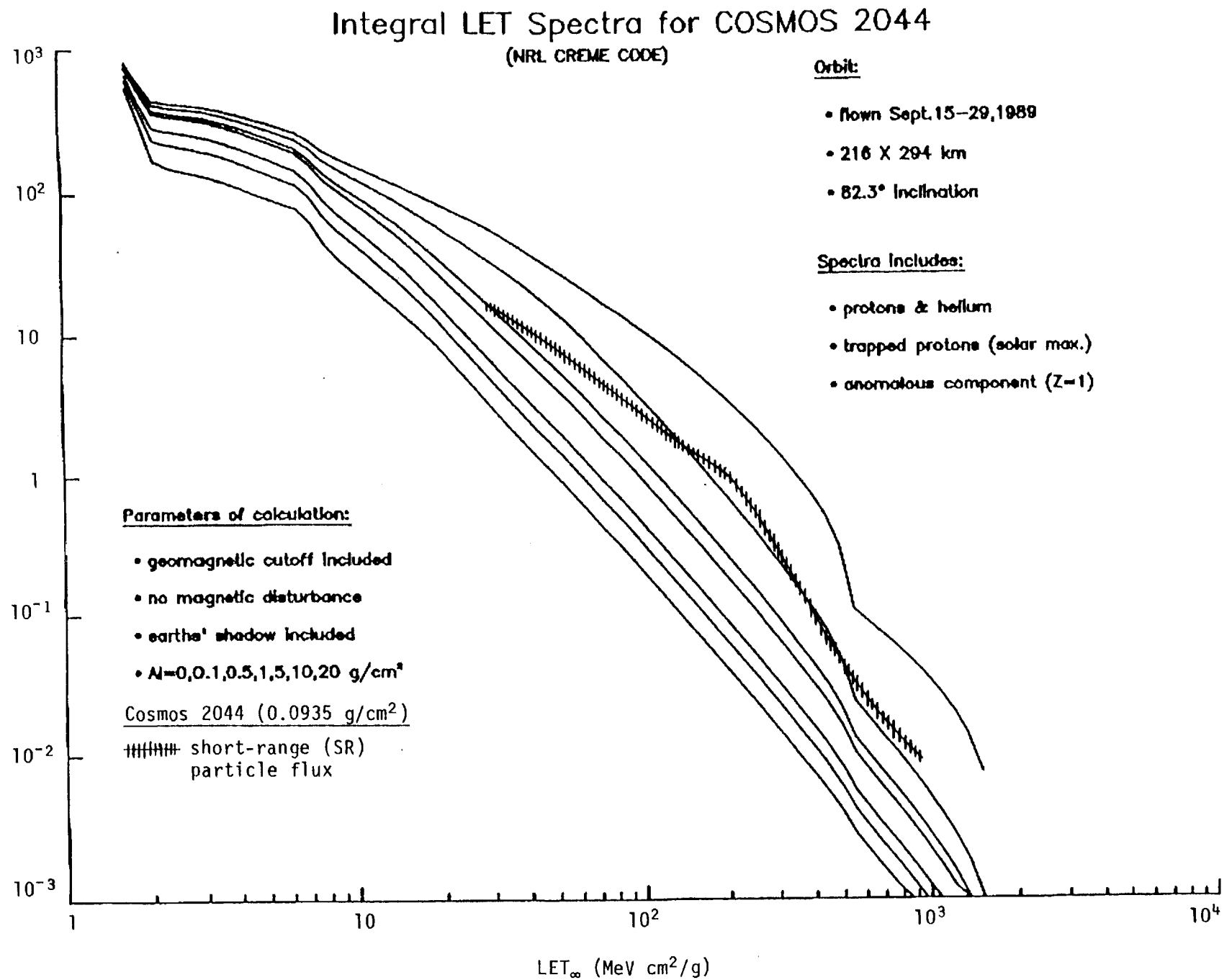

Fig. 26. Comparison of a measured Cosmos 2044 SR flux spectrum (in H_2O) with the calculated spectra (in Si) of John Watts /1990/ for Al shielding of 0–20 g/cm² and for the Cosmos 2044 orbit.

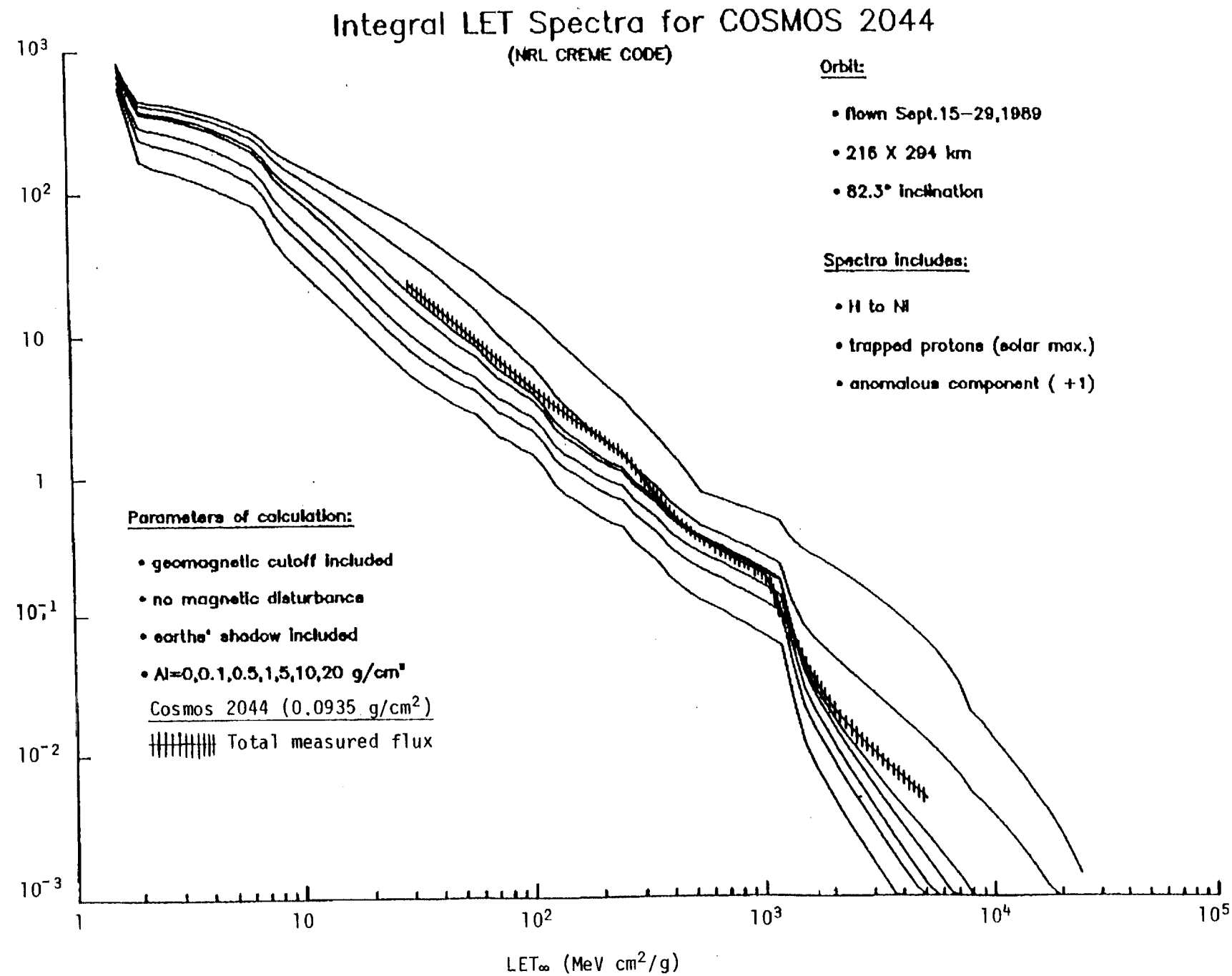

Fig. 27. Comparison of a measured Cosmos 2044 Total flux spectrum (in H_2O) with the calculated spectra (in Si) of John Watts /1990/ for Al shielding of 0–20 g/cm² and for the Cosmos 2044 orbit.

REFERENCES

Benton, E.V., Peterson, D.D., Bailey, J.V. and Parnell, T.A. (1977a), High-LET exposure of Skylab astronauts, *Hlth. Phys.* **32**, 15-20.

Benton, E.V., Henke, R.P. and Peterson, D.D. (1977b), Plastic nuclear track detector measurements of high-LET particle radiation on Apollo, Skylab, and ASTP space missions, *Nucl. Track Det.* **1**, 27-32.

Benton, E.V., Cassou, R.M., Frank, A.L., Henke R.P. and Peterson, D.D. (1978a), Experiment K206: Space radiation dosimetry on board Cosmos 936–U.S. portion of Experiment K206, in: Final Reports of U.S. Experiments Flown on the Soviet Satellite Cosmos 936 (Rosenzweig, S.N. and Souza, K.A., eds.) NASA TM 78526.

Benton, E.V., Peterson, D.D., Marenny, A.M. and Popov, V.I. (1978b), HZE particle radiation studies aboard Cosmos 782, *Hlth. Phys.* **35**, 643-648.

Benton, E.V., Henke, R.P., Frank, A.L., Johnson, C.S., Cassou, R.M., Tran, M.T. and Etter, E. (1981), Experiment K309: Space radiation dosimetry aboard Cosmos 1129: U.S. portion of experiment, in: Final Reports of U.S. Plant and Radiation experiments flown on the Soviet satellite Cosmos 1129 (Heinrich, M.R. and Souza, K.A., eds.), NASA TM 81288.

Benton, E.V. and Henke, R.P. (1983), Radiation exposures during spaceflight and their measurement, *Adv. Space Res.* **3**, No. 8, 171-185.

Benton, E.V. (1984), Summary of current radiation dosimetry results on manned spacecraft, *Adv. Space Res.* **4**, 153-160.

Benton, E.V., Frank, A.L., Parnell, T.A., Watts, J.W., Jr. and Gregory, J.C. (1985), Radiation environment of Spacelab-1, American Inst. of Aeronautics and Astronautics conference, *AIAA Shuttle Environment and Operations II*, Houston, TX, Nov. 13–15.

Benton, E.V. (1986), Summary of radiation dosimetry results on U.S. and Soviet manned spacecraft, *Adv. Space Res.*, **6**, No. 11, 315-328.

Benton, E.V. and Parnell, T.A. (1988), Space radiation dosimetry on U.S. and Soviet manned missions, in: *Terrestrial Space Radiation and its Biological Effects*, P.E. McCormack, C.E. Swenberg and H. Buecker, eds., NATO ASI Series A, Life Sciences 154, N.Y.: Plenum Press, pp. 729-794.

Benton, E.V., Frank, A.L., Benton, E.R., Dudkin, V.E. and Marenny, A.M. (1988), Radiation Experiments on Cosmos 1887, University of San Francisco, USF-TR-74.

Dobson, P.N., Jr. and Midkiff, A.A. (1970), Explanation of supralinearity in thermoluminescence of LiF in terms of the interacting track model, *Hlth. Phys.* **18**, 571-573.

Gorbics, S.G., Attix, F.H. and Kerris, K. (1973), Thermoluminescent dosimeters for high-dose applications, *Hlth. Phys.* **25**, 499-506.

Kovalev, E.E., Benton, E.V. and Marenny, A.M. (1981), Measurement of LET spectra aboard Cosmos 936 biological satellite, *Rad. Prot. J.* **1**, 169-173.

NASA-Space Life Sciences Payloads Office (1989), ATR-4 Ambient Temperature Recorder, Doc. No. A7SP-8801-D1, Ames Research Center, Moffet Field, California.

Peterson, D.D., Benton, E.V. and Tran, M. (1978), K103: HZE particle dosimetry, in: Final Reports of U.S. Experiments Flown on the Soviet Satellite Cosmos 782,(Rosenzweig, S.N. and Souza, K.A., eds.), NASA TM 78525.

Watts, J.W., Jr. (1988, 1990), Marshall Space Flight Center, Huntsville, Alabama, private communication.